SJSU SAN JOSÉ STATE UNIVERSITY

MTI MINETA TRANSPORTATION INSTITUTE

Structural Identification and Damage Detection in Bridges Using Wave Method and Uniform Shear Beam Models: A Feasibility Study

Mehran Rahmani, PhD, PE
Manan Naik, MSCE, EIT

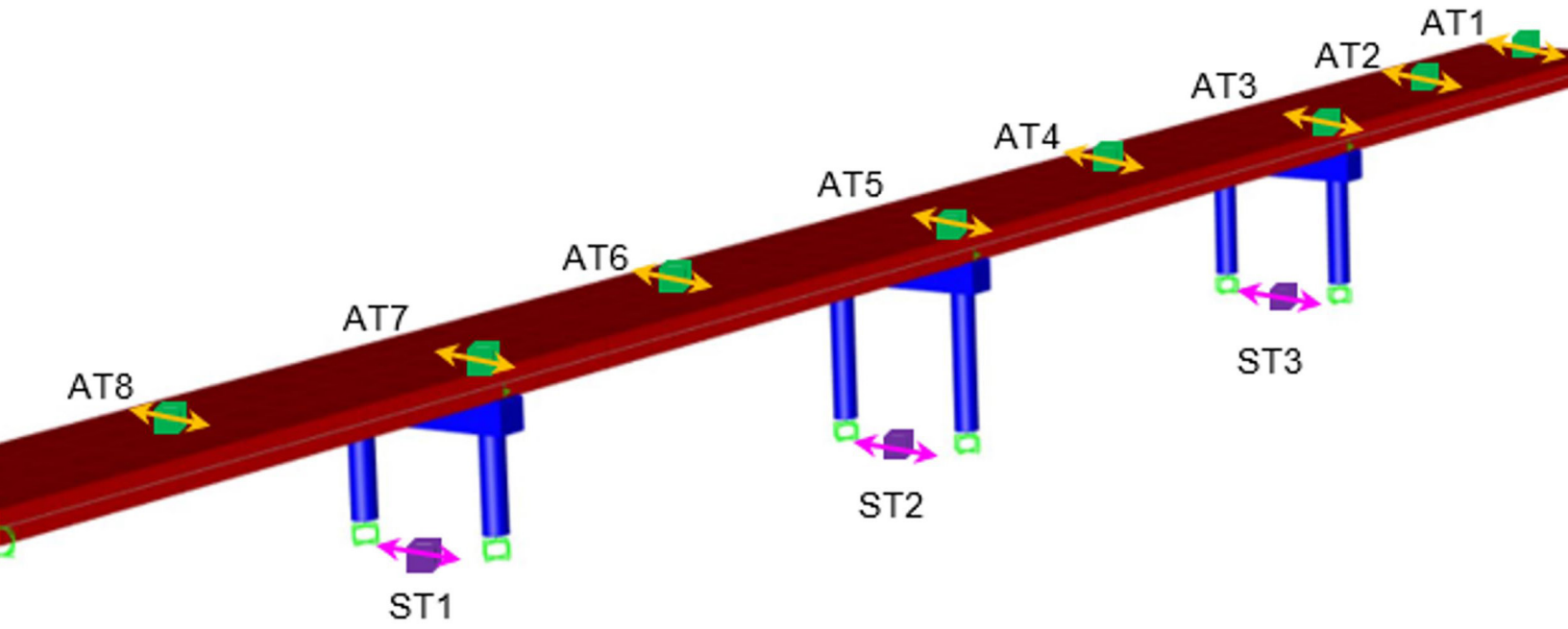

California State University Transportation Consortium

CALIFORNIA STATE UNIVERSITY LONG BEACH

Mineta Transportation Institute

Founded in 1991, the Mineta Transportation Institute (MTI), an organized research and training unit in partnership with the Lucas College and Graduate School of Business at San José State University (SJSU), increases mobility for all by improving the safety, efficiency, accessibility, and convenience of our nation's transportation system. Through research, education, workforce development, and technology transfer, we help create a connected world. MTI leads the Mineta Consortium for Transportation Mobility (MCTM) funded by the U.S. Department of Transportation and the California State University Transportation Consortium (CSUTC) funded by the State of California through Senate Bill 1. MTI focuses on three primary responsibilities:

Research

MTI conducts multi-disciplinary research focused on surface transportation that contributes to effective decision making. Research areas include: active transportation; planning and policy; security and counterterrorism; sustainable transportation and land use; transit and passenger rail; transportation engineering; transportation finance; transportation technology; and workforce and labor. MTI research publications undergo expert peer review to ensure the quality of the research.

Education and Workforce

To ensure the efficient movement of people and products, we must prepare a new cohort of transportation professionals who are ready to lead a more diverse, inclusive, and equitable transportation industry. To help achieve this, MTI sponsors a suite of workforce development and education opportunities. The Institute supports educational programs offered by the Lucas Graduate School of Business: a Master of Science in Transportation Management, plus graduate certificates that include High-Speed and Intercity Rail Management and Transportation Security Management. These flexible programs offer live online classes so that working transportation professionals can pursue an advanced degree regardless of their location.

Information and Technology Transfer

MTI utilizes a diverse array of dissemination methods and media to ensure research results reach those responsible for managing change. These methods include publication, seminars, workshops, websites, social media, webinars, and other technology transfer mechanisms. Additionally, MTI promotes the availability of completed research to professional organizations and works to integrate the research findings into the graduate education program. MTI's extensive collection of transportation-related publications is integrated into San José State University's world-class Martin Luther King, Jr. Library.

Report 21-02

Structural Identification and Damage Detection in Bridges using Wave Method and Uniform Shear Beam Models: A Feasibility Study

Mehran Rahmani, PhD, PE
Manan Naik, MSCE, EIT

February 2021

A publication of the
Mineta Transportation Institute
Created by Congress in 1991

College of Business
San José State University
San José, CA 95192-02

TECHNICAL REPORT DOCUMENTATION PAGE

1. Report No. 21-02	**2. Government Accession No.**	**3. Recipient's Catalog No.**
4. Title and Subtitle Structural Identification and Damage Detection in Bridges using Wave Method and Uniform Shear Beam Models: A Feasibility Study		**5. Report Date** February 2021 **6. Performing Organization Code**
7. Authors Mehran Rahmani, PhD, PE Manan Naik, MSCE, EIT		**8. Performing Organization Report** CA-MTI-1934
9. Performing Organization Name and Address Mineta Transportation Institute College of Business San José State University San José, CA 95192-0219		**10. Work Unit No.** **11. Contract or Grant No.** ZSB12017-SJAUX
12. Sponsoring Agency Name and Address State of California SB1 2017/2018 Trustees of the California State University Sponsored Programs Administration 401 Golden Shore, 5th Long Beach, CA 90802		**13. Type of Report and Period Covered** Final Report **14. Sponsoring Agency Code**
15. Supplemental Notes 10.31979/mti.2021.1934		

16. Abstract

This report presents a wave method to be used for the structural identification and damage detection of structural components in bridges, e.g., bridge piers. This method has proven to be promising when applied to real structures and large amplitude responses in buildings (e.g., mid-rise and high-rise buildings). This study is the first application of the method to damaged bridge structures. The bridge identification was performed using wave propagation in a simple uniform shear beam model. The method identifies a wave velocity for the structure by fitting an equivalent uniform shear beam model to the impulse response functions of the recorded earthquake response. The structural damage is detected by measuring changes in the identified velocities from one damaging event to another. The method uses the acceleration response recorded in the structure to detect damage. In this study, the acceleration response from a shake-table four-span bridge tested to failure was used.

Pairs of sensors were identified to represent a specific wave passage in the bridge. Wave velocities were identified for several sensor pairs and various shaking intensities are reported; further, actual observed damage in the bridge was compared with the detected reductions in the identified velocities. The results show that the identified shear wave velocities presented a decreasing trend as the shaking intensity was increased, and the average percentage reduction in the velocities was consistent with the overall observed damage in the bridge. However, there was no clear correlation between a specific wave passage and the observed reduction in the velocities. This indicates that the uniform shear beam model was too simple to localize the damage in the bridge. Instead, it provides a proxy for the overall extent of change in the response due to damage.

17. Key Words Structural Health Monitoring, Bridge, Accelerometer, Damage, Waves	**18. Distribution Statement** No restrictions. This document is available to the public through The National Technical Information Service, Springfield, VA 22161.		
19. Security Classif. (of this report) Unclassified	**20. Security Classif. (of this page)** Unclassified	**21. No. of Pages** 71	**22. Price**

Form DOT F 1700.7 (8-72)

DOI: 10.31979/mti.2021.1934

Mineta Transportation Institute
College of Business
San José State University
San José, CA 95192-0219

Tel: (408) 924-7560
Email: mineta-institute@sjsu.edu

transweb.sjsu.edu/research/1934

Acknowledgments

This research was supported by the California State University, Long Beach TRANSPORT 2018–2019 grant. The grant was made available to the university through seed grants from California State University Transportation Consortium (CSUTC), an appropriation through California's Senate Bill One (SB 1). The authors are grateful to the review panel members and the College of Engineering research and grant administration personnel.

The sensory data used in this report were provided by the University of Nevada, Reno, and downloaded via the Digital Environment for Enabling Data-Driven Science (DEEDS) at datacenterhub.org.

Contents

List of Figures

List of Tables

Executive Summary

This report presents a wave method to be used for the structural identification and damage detection of structural components in bridges, e.g., bridge piers. This method was shown by Rahmani and Todorovska (2013) to be promising when applied to real structures and large amplitude responses in buildings (e.g., mid-rise and high-rise buildings). The present study is the first application of the method to bridge structures. The bridge identification was performed using wave propagation in a simple uniform shear beam model. The method identifies a wave velocity for the structure by fitting an equivalent uniform shear beam model to the impulse response functions of the recorded earthquake response. The structural damage is detected by noting changes in the identified velocities from one damaging event to another. The method uses the acceleration response of a shake-table four-span bridge tested to failure for detecting change in the structure. The availability of the shake-table test data provided an opportunity to check the accuracy of the uniform shear beam model identification results. It also revealed the strength and limitations of the shear beam model for damage detection in bridges.

The prototype bridge was instrumented using nine triaxial accelerometers at the deck level and three triaxial accelerometers at the base of its columns (i.e., shake-tables). A uniform shear beam model can be identified using data from two channels (source and receiver). Unlike building structures which typically comprise sensors placed on their floors (along their height), the sensor placement on a bridge involves a two-dimensional distribution (along the height and length of the bridge). Therefore, two scenarios for wave propagation in the bridge were proposed. In each scenario, pairs of sensors were identified to represent a specific wave passage in the bridge. Identified wave velocities for each scenario and for various shaking intensities were reported. A summary of actual observed damages in the structure was prepared. The observed damages were then grouped into five damage states. Further, damage states were compared with the detected reductions in the identified velocities. The results show that: (1) the identified shear wave velocities presented a decreasing trend as the shaking intensity was increased, (2) the percentage reduction in the velocities was consistent with the overall observed damage in the bridge; and (3) there was no clear correlation between a specific wave passage and the observed reduction in the velocities. This indicates that the uniform shear beam model was too simple to localize the damage in the bridge. It rather provides a proxy on the extent of complete change in the response due to damage.

While the shear beam model provided a unique opportunity to extend the wave method application to bridge structures, the investigation revealed that a more detailed model will be required to take into account the bending nature of bridge responses and the significant wave dispersion associated with it. Further study will be needed to develop and calibrate a more detailed model for the purpose of robust damage detection and damage localization in bridges.

I. Introduction

1.1 Problem Statement and Objectives

Structural health monitoring (SHM) is a process of determining changes in a structure over a period of time and detecting damage in it. Damage is defined as the change in the physical properties of a building or bridge which affects the overall response of the structure. In recent times, the number of bridges is growing rapidly in metro cities as well as mega cities. It becomes very difficult to monitor every bridge during or after an earthquake event has occurred. It is time-consuming to visually inspect a bridge, as it can take up to several weeks to determine the damage. Larger bridges, specifically, require a longer inspection time.

SHM can enable engineers to monitor bridge responses over a period of time with the help of various sensors placed on the structure. The sensory data can potentially help detect damage soon after an earthquake strikes. SHM also saves a large amount of money and time, since emergency responders do not have to inspect the entire bridge structure after a major earthquake. Therefore, we should try to build smart bridges instrumented by various sensors (e.g., strain gauges, accelerometers, etc.) during or after construction. Earthquake impact depends on several factors such as the structural system of the bridge, the shaking intensity, and distance from the earthquake epicenter; these impacts greatly affect the response of a bridge, and the responses are recorded by sensors.

Figure 1 shows the main components of structural health monitoring. The system consists of collecting raw data using a number of sensors along the bridge, processing the data, applying a robust methodology to identify changes in the bridge, and finally making decisions based on these changes. The methodology is a key factor for a successful damage detection: it interprets the recorded response of a bridge (e.g., deck acceleration) as useful information to make a correct decision.

Using data from the sensors, researchers can monitor the response of the bridge from a remote location during or after an earthquake. The smaller and less expensive sensors are installed at various locations to capture the structural vibration. Many bridges in California are instrumented by several accelerometers. Data from these full-scale bridges are valuable for developing a robust SHM methodology and calibrating these methods.

This project develops a methodology for structural health monitoring, known as the wave method, for bridge structures. The method proved to be a robust and reliable method for buildings (Rahmani et al. 2015), for instance, when applied to large responses of a 12-story reinforced concrete building. This research extends the application of the SHM method from building to bridge structures. It explores the feasibility of the method for SHM in bridges—and further, the possibility of its adoption in a seismic alert system in metropolitan areas. The SHM process in this study includes identifying the responses of the case-study bridge using wave propagation in a

simple uniform shear beam model. The method also involves identifying a wave velocity for the structure by fitting an equivalent uniform shear beam model to the impulse response functions of the recorded earthquake response. The structural damage was inferred by detecting changes in the identified velocities from one damaging event to another.

To further understand the dynamic behavior of the bridge and to investigate the wave method's results, a linear Finite Element Model (FEM) of the bridge was created using SAP2000 software. The structural drawings and geometric details of the bridge were obtained from the original project report on the tested bridge (Nelson et al. 2007); we updated the properties of the model so that the response of the FEM would best match the recorded data from the actual bridge in the linear domain. The updated FEM was subjected to two earthquakes at its base. The input accelerations were taken from the recorded response at the shake-table level. Linear time history analysis was carried out for the displacement and acceleration response at different sensors' locations. Chapter III mainly discusses the process of updating the model and the findings.

Chapter IV includes the main results of this study. It provides details of the shear beam model fitted to the observed response of the bridge, a summary of the visual damage survey of the bridge, and a discussion of the accuracy of the wave method for detecting damage in the bridge from one damaging motion to another.

Figure 1. Components of Structural Health Monitoring (SHM),
Adopted from M. Rahmani 2014

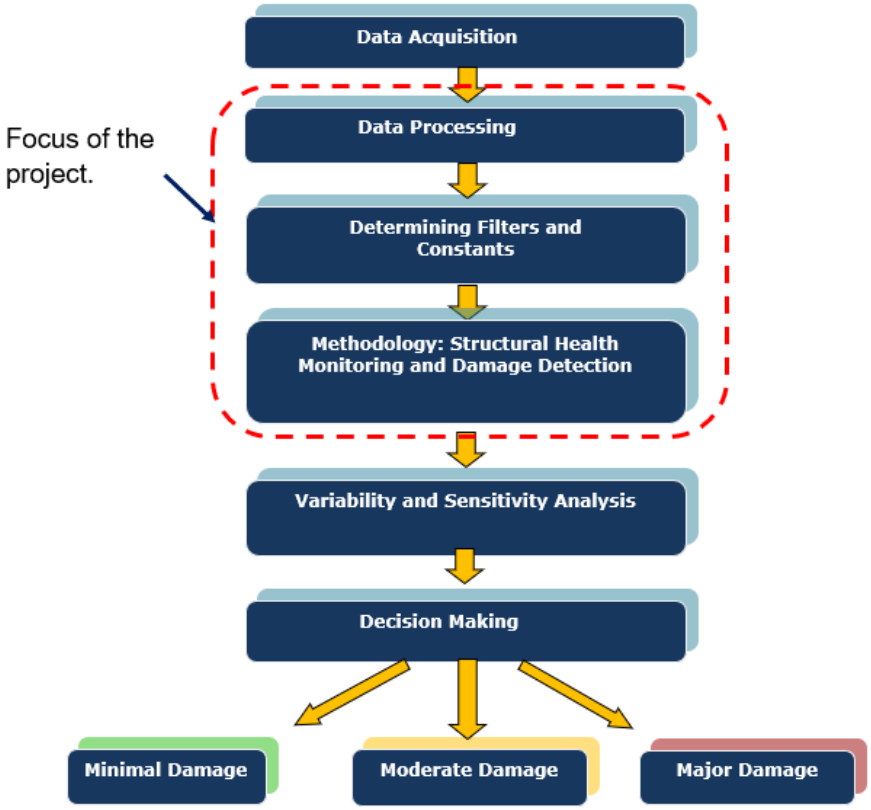

1.2 Wave Methods for Structural Health Monitoring

The seismic response of the bridges is generally seen as a vibrational process but can alternatively be seen as a wave propagation process. In the case of buildings, it has been shown that the damage can be detected if a change is noticed in the velocity of the waves propagating vertically through the structure (Todorovska and Rahmani 2012; Rahmani et al. 2015).

This study investigates the feasibility of applying the wave method to bridge structures. The analytical wave propagation model utilized for modeling the bridge structure is based on a simple uniform shear beam (Todorovska and Rahmani 2012). The medium is assumed to be isotropic and homogeneous in the case of a uniform shear beam. The beam is characterized by its height, mass density ρ, and shear modulus μ. The shear wave velocity can be calculated using the beam's properties as

$$c = \sqrt{\mu/\rho}.$$

Within the beam, the wave can propagate from a reference point (sensing station A) to a receiving point (sensing station B) along the beam. Using the response of the beam (e.g., acceleration), an impulse response function (IRF) of a low-pass filtered signal can be calculated by means of an inverse Fourier transform of the Transfer Functions (TFs) at the sensing stations. Analytical IRFs were derived by Todorovska and Rahmani (2012) for a uniform shear beam model. The IRF at the reference point is essentially a sinc function (single pulse with unit amplitude), while at the receiving station it presents an attenuated main pulse and its reflections from the beam's boundaries. It was shown by Todorovska and Rahmani (2012) that if the location of the reference station is chosen to be on the structure's actual physical excitation level (e.g., its foundation level), all propagating pulses at the receiving station will occur at positive times. In contrast, if the reference station is selected at a level other than the actual input excitation level (e.g., at deck level or roof level), the propagating pulses at the receiving station (which can be the actual excitation level) occur both in positive time (causal pulses) and in negative time (acausal pulses). In the latter case, the reference station is referred to herein as the virtual source.

The bridge dynamic characteristics are identified by fitting the analytical IRFs of a uniform shear beam model to the observed IRFs for the actual bridge. The observed IRFs and TFs are calculated from the recorded acceleration response of the actual tested bridge. Figure 2 illustrates the analytical IRF for a three-layer model of a nine-story building in Pasadena, California, excited by the 2002 Yorba Linda earthquake and with the virtual source at roof level (Rahmani and Todorovska 2013).

Figure 2. Impulse Response Functions at each Floor for the Three-Layer Model, for Virtual Source at Roof, Millikan Library (adopted from Rahmani and Todorovska 2014)

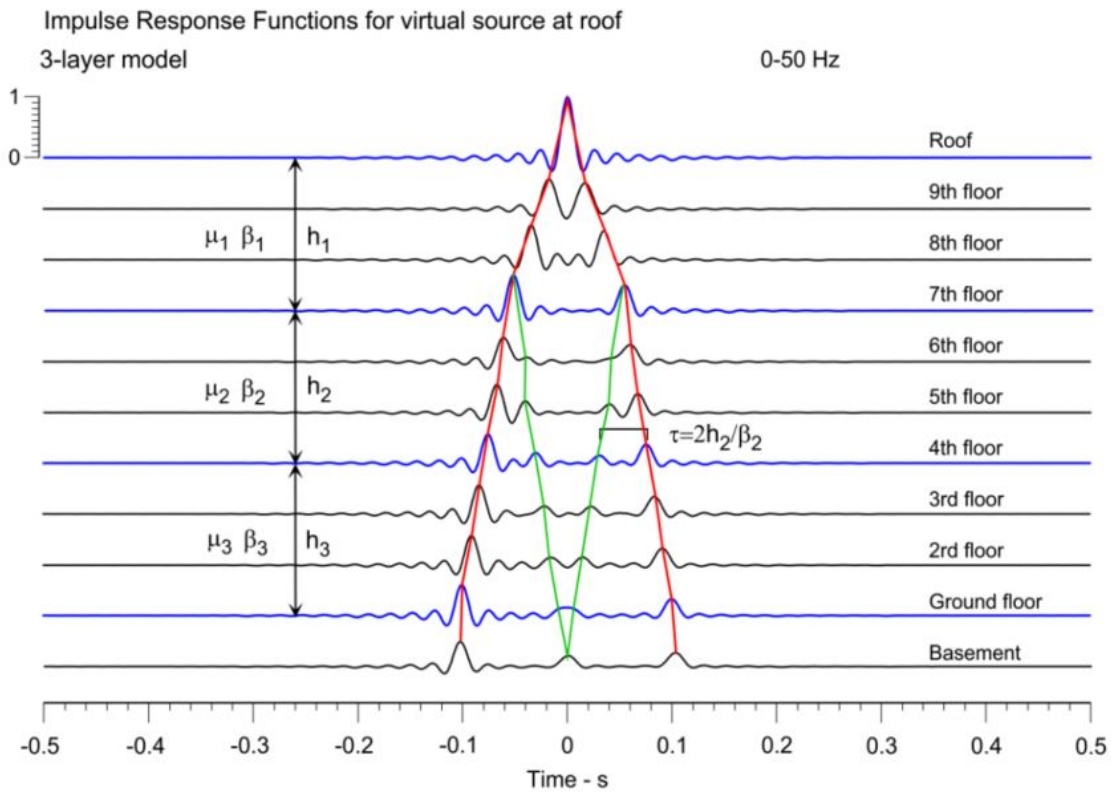

1.3 Organization of This Report

The wave-based methodology for structural identification is discussed in more detail in Chapter II. Chapter III presents the process of creating and updating the linear FEM of the bridge, which also includes the details and geometry of the bridge, load effects, and post processing of recorded acceleration responses. This section goes more in depth to compare the linear time history response and modal frequencies during two of the input excitations. Chapter IV presents the research team's main attempts to identify the bridge structure during various input excitations and to infer the onset of structural damage from the results. Seven input excitations were utilized; each represented a state of damage in the bridge. As part of the identification algorithm, the research team introduced two scenarios for the wave passage in the bridge. A detailed discussion is presented regarding the identified shear wave velocity, percentage of change in velocity, and the velocity reduction trend among the bents. Chapter V presents the main findings and conclusions as well as proposed work to be implemented in the future.

II. Methodology

2.1 Seismic Interferometry

The wave method falls under the category of seismic interferometry techniques where the properties of the physical domain between two points are estimated using the recorded seismic signals at the two points (i.e., stations). The response of the bridge is modelled using a viscously damped shear beam. A uniform shear beam model has been identified in this study. Shear waves propagate vertically in the beam from a source station to a receiving station. The medium is assumed to be homogeneous and isotropic within the uniform shear beam. The shear beam is characterized by height h, mass density ρ, and shear modulus μ which relate to the shear wave velocity (c) through the following expression (Rahmani and Todorovska 2013):

$$c = \sqrt{\mu/\rho}.$$

The damping ratio is defined by

$$\zeta = \frac{1}{2Q}.$$

Q is the quality factor accounting for reductions of the pulse amplitude due to material damping.

Within the structure, a wave can propagate from a reference point (sensing station A) to a receiving point (sensing station B) along the bridge. Let the transfer functions (TF) and impulse response functions (IRF) be as follows (Rahmani and Todorovska 2013):

TF: $\hat{h}(z, 0; \omega)$ computed at any level z (measured from the deck downwards) wrt deck motion;

IRF: $\hat{h}(z, 0, \omega_{max}; t)$ computed by the inverse Fourier transform of the TF, shown below.

$$\hat{h}(z, 0; \omega) = \frac{\hat{u}(z,\omega)\bar{\hat{u}}(0,\omega)}{|\hat{u}(0,\omega)|^2+\varepsilon}$$

$$h(z, 0, \omega_{max}; t) = \frac{1}{2\pi}\int_{-\omega_{max}}^{\omega_{max}} \hat{h}(z, 0; \omega)e^{-i\omega t}d\omega$$

in which ε is the regularization parameter and ω_{max} is the cut-off frequency of the low-pass filter.

Then,

$$\omega_{max} = 2\,\pi\, f_{max}$$

is considered as the most valuable fit parameter which controls the width of the source pulse per Rahmani and Todorovska (2012). The IRF at the reference point is essentially a sinc function (single pulse with unit amplitude), while at the receiving station it presents an attenuated main pulse and its reflections from the beam's boundaries. It was shown by Todorovska and Rahmani

(2012) that if the reference station is selected at a level other than the actual input excitation level (e.g., reference selected at deck level or at roof level), the propagating pulses at the receiving station (e.g., foundation level which is the actual excitation level) occur both in positive time (causal pulse) and in negative time (acausal pulse). In this case, the reference station is referred to as the virtual source.

2.2 Waveform Inversion Algorithm: An Overview

The identification algorithm used in this report involves the fitting of pulses in the IRF over predefined time windows. The *observed* IRFs are computed from the recorded acceleration responses, while the *model* IRFs are computed from the propagator of the analytical shear beam. The fitting of the model IRFs to the observed IRFs are performed in the least square sense. For the nonlinear least square regression, we use the Levenberg-Marquardt method via the MATLAB program. This algorithm was shown to be robust to directly fit the causal and acausal pulses and estimate the beam's shear wave velocity. We try to fit both the causal and acausal pulses but not the ripples in between the pulses which are caused by the waves' reflections from the boundaries and are heavily affected due to wave dispersion in the structure. Figure 3 shows an example of fitting the IRFs for a tall building at different stations along building height. The process of fitting is carried out for several pairs of sensors defined in our wave passage scenarios (discussed in Chapter IV). The identification results which include shear wave velocities in the fitted beam models are organized and their changes are discussed and compared with actual damage in the bridge.

Figure 3. Example of Wave-Based Identification Algorithm Fitting Impulse Response Function (Rahmani and Todorovska 2013)

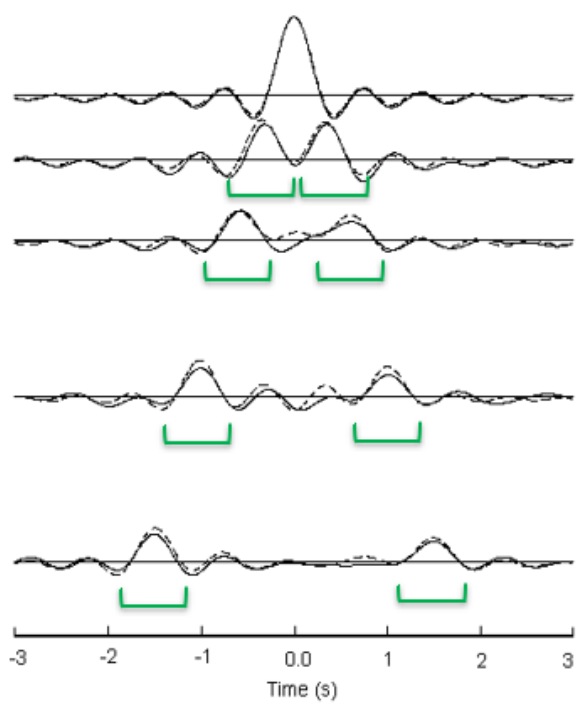

2.3 Structural System of the Bridge

Layout of Accelerometers and Displacement Sensors

There are various sensors installed along the case study bridge and on different components. The sensors recorded accelerations and displacements of the bridge. Superstructure accelerometer sensors account for 22 channels of acceleration data collection. The channels were oriented in the longitudinal, transverse, and vertical directions. The sensors were located atop columns, at the mid length of each span, and at the north and south end of a bridge; this takes care of the longitudinal (north-south) and transverse (east-west) directions to measure accelerations as well as displacements, though only the acceleration and displacements in the transverse (east-west) direction were utilized for identification and modeling purposes. The vertical accelerations were measured at the mid-point of each span. The bridge is subjected to seven biaxial motions (transverse motions and longitudinal motions combined). The research team is particularly interested in identifying the damage using the transverse response of the bridge deck.

There are nine displacement sensors along the bridge measuring the displacement in the transverse direction. The displacements were measured at the location exactly above the column, at the mid length of each span and at the north and south ends of the bridge. The displacement sensors at the north and south ends of the bridge measures the deck displacement in the longitudinal direction. In this study, the acceleration and displacements only in the transverse (east-west) direction were utilized for identification and modeling purposes.

Table 1. Placement of Sensors in the FEM Equivalent to Sensors' Layout in the Bridge

Location of Acceleration Sensors on the Bridge

Sensor	Joint in SAP2000	Sensor	Joint in SAP2000
AT1	368	AT7	3
AT2	63	AT8	67
AT3	46	AT9	90
AT4	55	ST1	416
AT5	23	ST2	422
AT6	56	ST3	433

Location of Displacement Sensors on the Bridge

Sensor	Joint in SAP2000	Sensor	Joint in SAP2000
DT1	2	DT7	46
DT2	74	DT8	62
DT3	3	DT9	57
DT4	75	ST1	416
DT5	23	ST2	422
DT6	36	ST3	433

Figures 4 and 5 present the location of sensors on the bridge from this investigation's Finite Element Model (FEM) of the bridge in SAP2000. The joint numbers are taken from the FEM of the bridge. The sensor outputs are based on the absolute accelerations and absolute displacements corresponding to global coordinates in the SAP2000 program.

Figure 4. Location of Acceleration Sensors on the Bridge in SAP2000

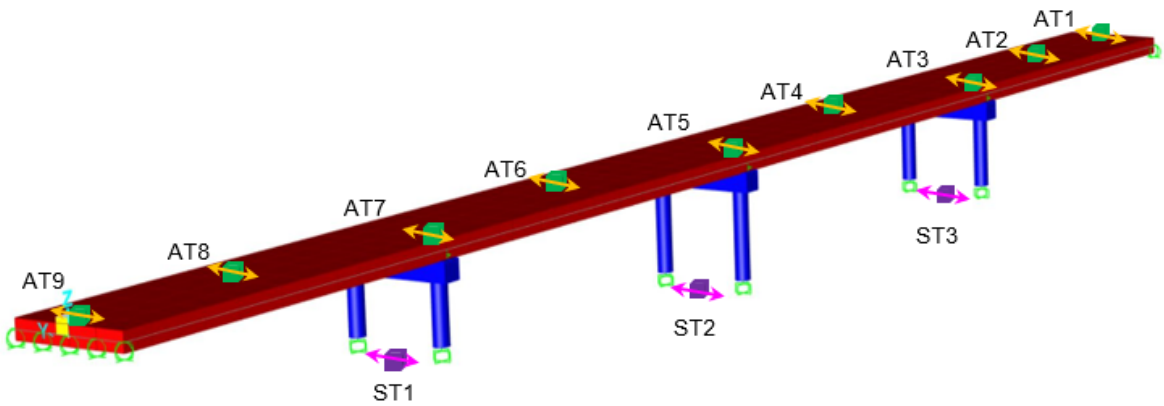

Figure 5. Location of Displacement Sensors on the Bridge in SAP2000

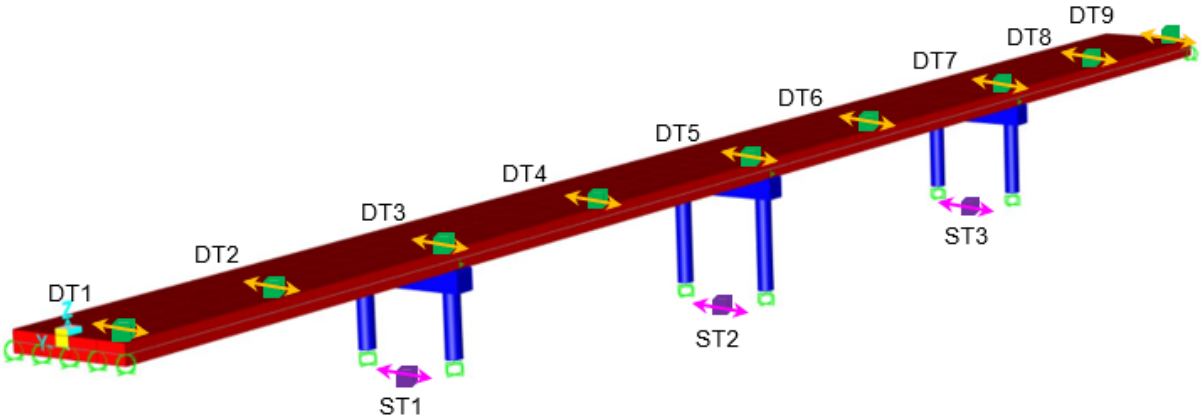

III. Linear Finite Element Model of the Bridge

3.1 Structural Details of the Bridge

The 107-ft-long bridge was modelled using SAP2000 software. The model was updated several times until the dynamic time history response of the bridge matched reasonably well with that observed in the tested bridge. The geometry of the bridge, weights of the blocks, location of the blocks, and compressive strength of the concrete were the key measures in the analysis of the bridge. Post-tensioning tendons at the deck levels were modeled in SAP2000 as well. The tendons changed the axial load distribution in the columns consistent with statements in the original report on the bridge (Nelson et al. 2007). Information and structural drawings pertaining to the bridge, deck, columns, bent cap, and tendons were obtained from the report (Nelson et al. 2007). Damping in the model was finalized by trials on the modeled bridge until the response of the model was close to the response from the recorded data.

After the model was complete, the time history response obtained using the linear direct integration was used to visualize and understand the response of the structure under the different earthquake motions. By means of the time history analysis, the deck accelerations and displacements were extracted at different sensor locations and compared with the observed bridge response. The FEM helped the research team to better understand the dynamic response of the tested bridge and its modal frequencies and shapes, in the linear domain, and to find the best strategies for the identification process using the wave method.

Geometry of the Bridge

The 107-ft tested bridge is a four-span continuous post-tensioned concrete flat slab. The two interior spans are 29 ft each while the two exterior spans are 24.5 ft each. The slab of the bridge is rectangular, having a width of 90 in and depth of 14 in. There are three bents consisting of two columns each. The heights of the columns in each bent varied with each other, making the bridge asymmetric. The heights of the columns were 5, 7, and 6 ft, respectively, with the tallest bent located in the middle. Figure 6 shows the layout of the bridge in the X-Z plane showing the varied heights of the bents.

Figure 6. Height of each Bent of the Bridge

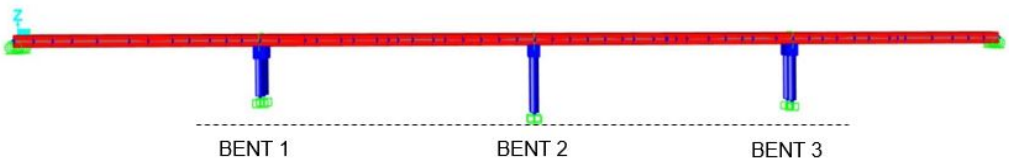

The cap beams' depth and length are 15 and 98 in, respectively. The columns are circular in shape with a diameter of 12 in. The initial modelling of bridge was done in CSi Bridge software. The compressive strength of concrete for the abutment, bent cap, and columns was taken as 5,700 psi. In our finite element model, the cracked section of the bent cap, columns, and deck were taken as $0.3I_g$, $0.35I_g$, and $0.3I_g$, respectively, according to the Caltrans Seismic Design Criteria Version 2.0 (2019). The abutments were modeled using simple roller supports. This decision was based on the fact that the bridge end supports were not shear keys and further that the present study only considered the transverse motion of the bridge. Comparing the fundamental frequency in the transverse direction showed reasonable agreement between the model and the actual bridge's dynamic response.

Applied Load Types and Magnitude on the Structure

The case study bridge had two different types of gravity loadings: dead load and superimposed dead load. These loads alter the modal response of the bridge. The dead load is generally the weight of the structure itself. Superimposed dead load in this study replicates the load from the traffic and pedestrians applied in the form of additional weight on the bridge structure such as with blocks and leads. On this structure, there were eight large blocks and four small blocks of (namely leads) placed on the bridge at different locations. The weight of these blocks was extracted from the data files provided on the datacenterhub (datacenterhub.org/dv_dibbs/view/1322). The weight of each big block was found to be 20 kips and the weight of each small block of leads was 8 kips. The first mode of vibration in the transverse direction, according to the original report by Nelson et al. (2007), was found to be 2.5 Hz. On the other hand, after the above loads were applied in the finite element model and the structure's response was analyzed, the first mode of the bridge model in the transverse direction measured at 2.62 Hz, which was found to be reasonably close to that of the actual bridge.

Modelling of Post-Tensioning Tendons

The modelling of the tendons was done in SAP2000. There were three tendons running from one end of the deck to the other along the bridge. The post-tensioning force of each duct was 205 kips with a 2.875-in diameter and tensile strength of 270 ksi.

After running the analysis in the SAP2000, the research team found that the axial dead load on the columns of Bent 1, Bent 2, and Bent 3 was 42.56 kips, 41.9 kips, and 42.78 kips, respectively, and the axial load of tendons on the columns was 12.29 kips, 17.56 kips, and 12.67 kips, respectively. The original report by Nelson et al. (2007) suggests that the unusual tendon path increased the load on the middle bent and lessened the load on the exterior bents. The researchers noticed the same trend in the present analysis, such that the final axial loads on the columns including the dead and post-tensioned load from the FEM were found to be 30.27 kips, 59.46 kips, and 30.11 kips. Comparing these forces with design forces in the original report revealed that the present values for the columns' axial dead loads are slightly different but follow the same ratios for side bents versus the middle bent. This difference is due to modelling error, as the correct path of the tendon was not known. Figures 7 and 8 show the tendon design on the bridge and an elevation view of the tendons.

Figure 7. Tendons' Path on the Bridge

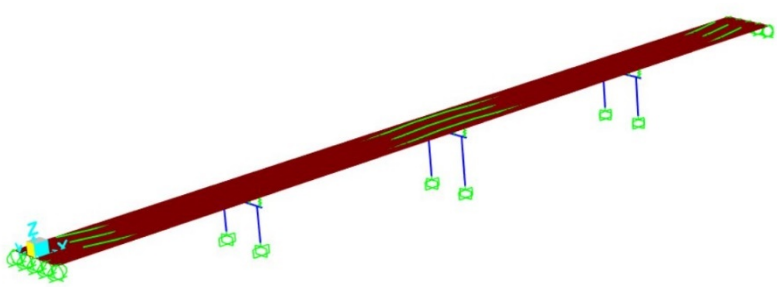

Figure 8. Elevation View of the Tendons

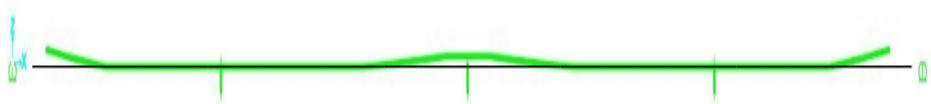

Post Processing of Recorded Acceleration Response

The recorded (i.e., observed) acceleration and displacement data from the sensors located on the bridge were obtained from data files uploaded on the NEES datacenterhub website. The raw acceleration and displacement data that were obtained had wavy baselines which in some cases started at a non-zero value of acceleration or displacement at t=0 second. Therefore, post processing of recorded acceleration was necessary to correct the baseline. The research team carried out this task using a customized MATLAB code. The raw data of all the sensors on the bridge were processed for the first 30 seconds for all the biaxial motions. The corrected acceleration at the shake-table level was then utilized as input excitation in the finite element model.

3.2 Model Updating Based on Two Recorded Earthquakes Motions

Linear Time History Response Analysis and Comparison

The FE model was subjected to two biaxial motions (Biaxial 1 and Biaxial 2) out of seven biaxials. Direct integration time history (TH) linear analyses were carried out for the two motions since their input excitations were small in amplitude and most likely resulted in a linear response in the bridge. The corrected acceleration time histories of the shake-tables 1, 2, and 3 were plotted on top of each other in the longitudinal and transverse directions to enable comparison between the three shake-tables. Figures 9 to 12 show that the motions at the three shake-tables are practically identical.

Figure 9. Shake-Tables Acceleration Time History during Biaxial 1 in Longitudinal Direction

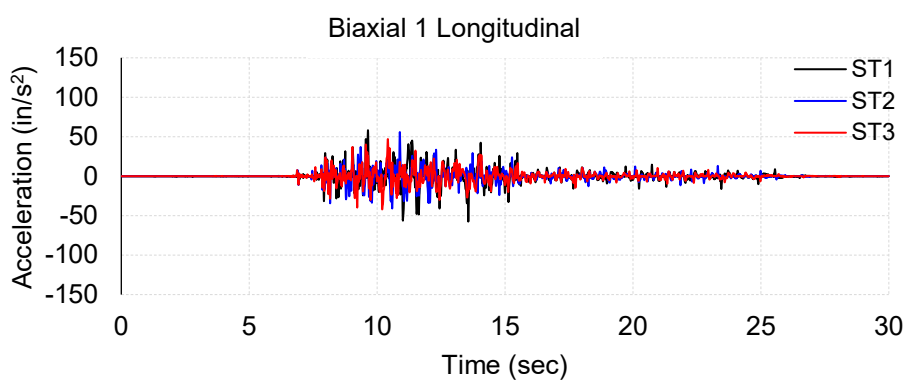

Figure 10. Shake-Tables Acceleration Time History during Biaxial 2 in Longitudinal Direction

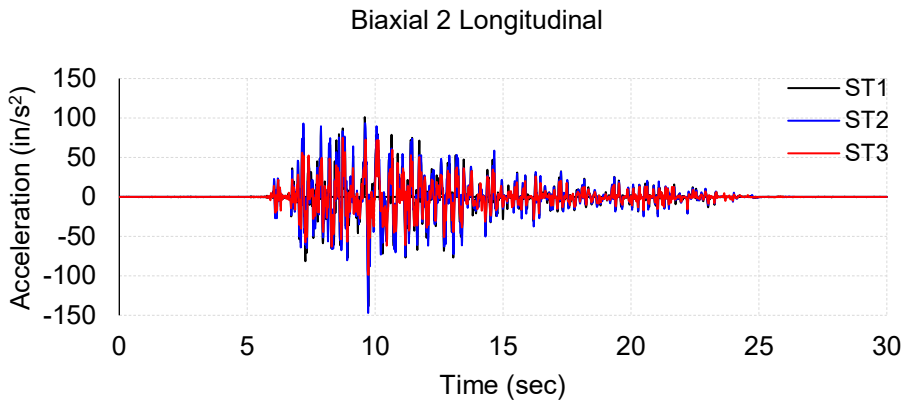

Figure 11. Shake-Tables' Acceleration Time History during Biaxial 1 in Transverse Direction

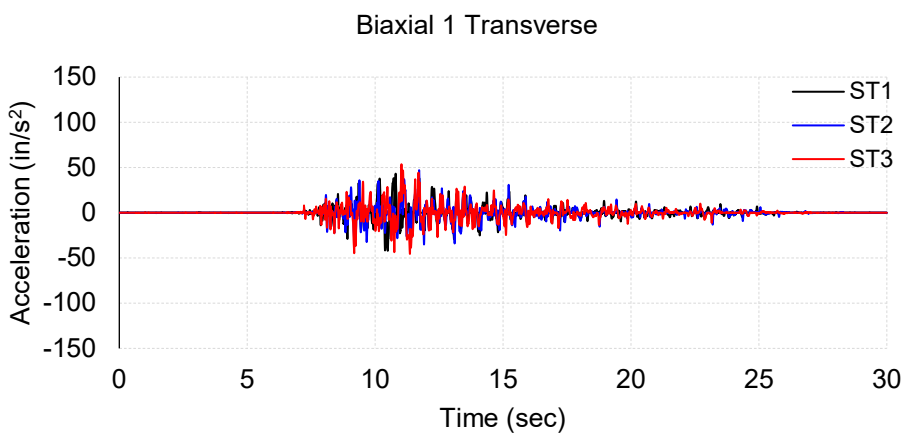

Figure 12. Shake-Tables' Acceleration Time History during Biaxial 2 in Transverse Direction

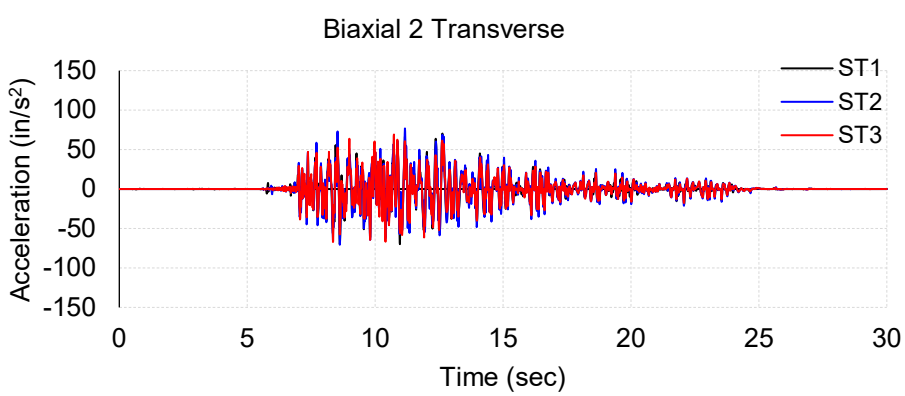

To draw a further conclusion about the input motions being identical, the frequency responses for the three shake-tables were computed. To do this, the Fourier spectra of the three shake-table motions were plotted on top of each other. Figures 13 to 16 show that the Fourier spectra remain identical for the three shake-tables (ST) in the longitudinal and transverse directions.

Figure 13. Fourier Spectra of the Shake-Table Motion during Biaxial 1 in Longitudinal Direction

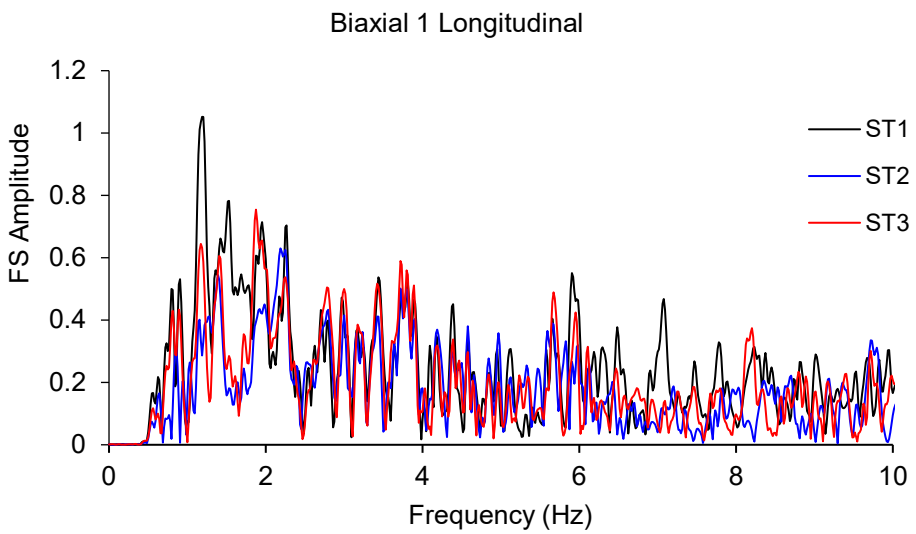

Figure 14. Fourier Spectra of the Shake-Table Motion during Biaxial 2 in Longitudinal Direction

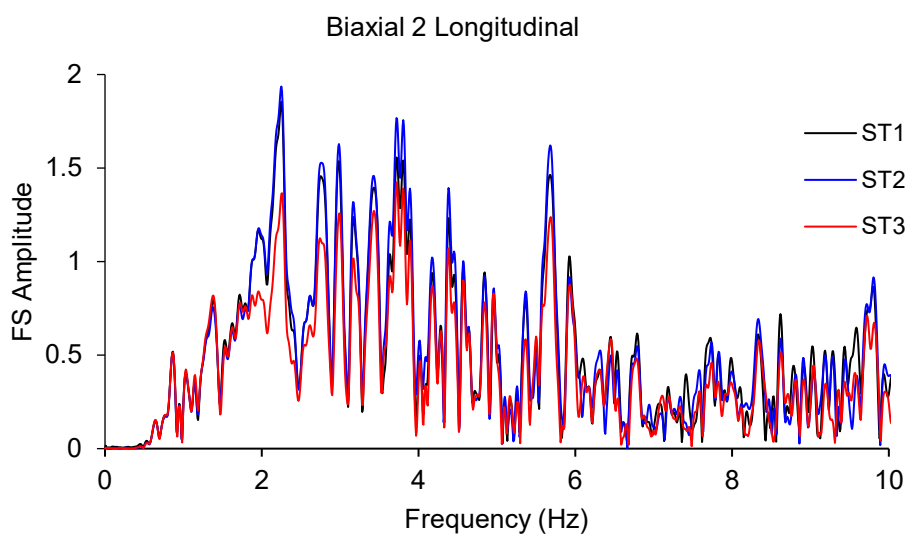

Figure 15. Fourier Spectra of the Shake-Table Motion during Biaxial 1 in Transverse Direction

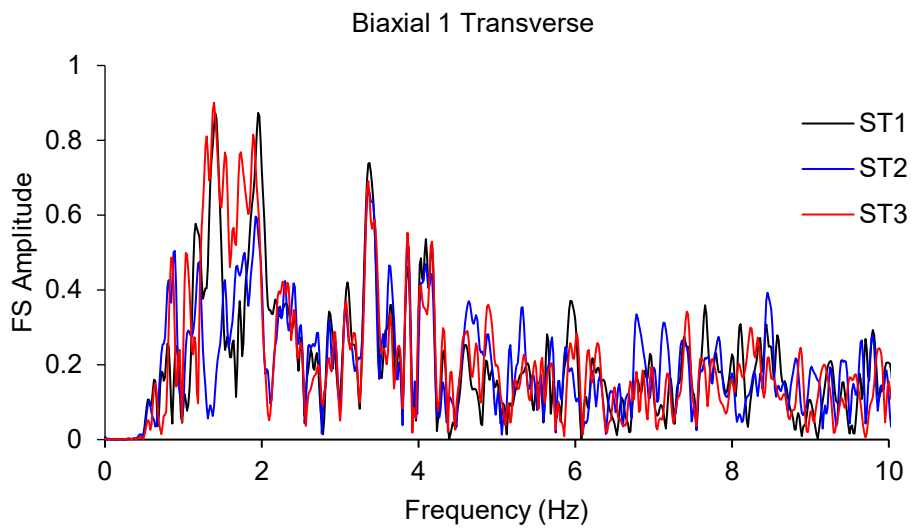

Figure 16. Fourier Spectra of the Shake-Table Motion during Biaxial 2 in Transverse Direction

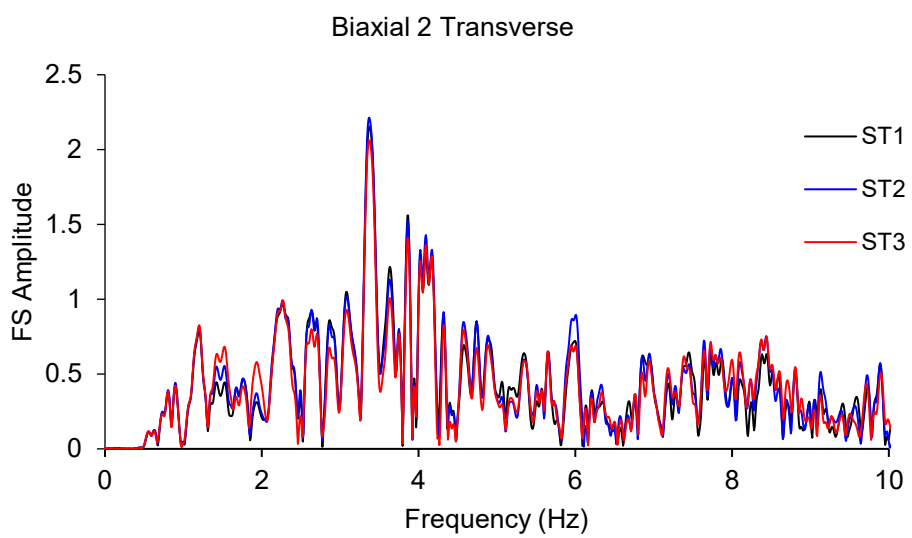

Looking at the shake-tables' acceleration time history plots and the Fourier spectra of Biaxial 1 and Biaxial 2 in the longitudinal and transverse directions, it is safe to conclude that all three shake-tables were excited identically. Hence, shake-table 2's corrected accelerations were imported into the SAP2000 model as base input motions in the longitudinal and transverse directions for the Biaxial 1 and 2 cases.

To compare the results for the deck acceleration and displacement, two different damping values were tried for the first and second vibrational modes. The approximate estimated damping value is 5.1%. Further, Rayleigh damping was utilized to approximate final damping values for input in the FEM. Rayleigh damping is proportional to the mass and stiffness of the bridge. Since the first

three modal frequencies lay within 0–10 Hz, the research team decided to utilize the first and ninth modes of vibration (1.2 and 10 Hz, respectively) to set limits for the Rayleigh damping coefficients.

Figure 17 shows the Rayleigh damping curve used in the finite element model where *a* and *b* represent α and β values taken to estimate damping properties of the model corresponding to the first and ninth modal frequencies (Chopra 2017). As shown in Figure 17, the damping ratios for the frequency range between 1 Hz to 10 Hz are reasonable. Two cases of damping were checked: 3–5% damping and 7–9% damping. A similar type of plot was generated and examined for each. After reviewing the response of the bridge, 3–5% damping was found to be suitable.

Figure 17. Rayleigh Damping Estimation used in the Finite Element Model (FEM)

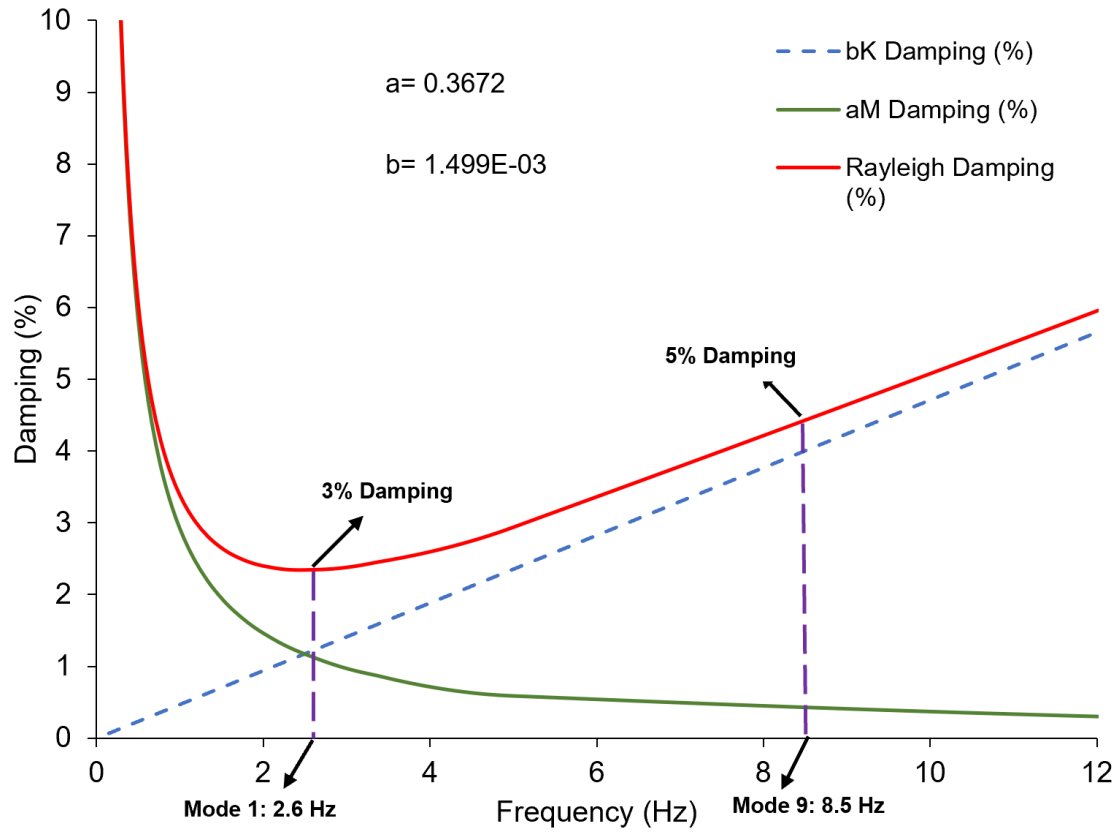

After the linear time history (TH) analysis had been run, the absolute accelerations and absolute displacements were computed at a specific node to compare the response of the FE model and the observed response.

The TH analysis was performed for the FEM by inputting the corrected accelerations for shake-table 2 at the base of all columns. The displacement response of the bridge was compared at selected transverse channels where displacement sensors were located. The comparison was made between the response from SAP2000 and that found in the observed data for a few sensors during

Biaxial 1 and Biaxial 2 separately. The observed data of the bridge were obtained from the NEES website.

The FEM output results showed inaccuracy after about 16 seconds for the Biaxial 1 and Biaxial 2 input motions: the displacement response was falling off from the zero baseline. In order to capture the correct displacement response, according to the SAP2000 manual, it was necessary to perform the baseline correction of FEM displacement data after 16 seconds. A polynomial order 4 was fitted for the baseline correction. Figures 18 to 21 show the baseline corrected plots for DT6 and DT7 for Biaxial 1 and Biaxial 2, respectively. The results show a reasonable agreement between the FEM and the actual bridge response.

Figure 18. Displacement TH Comparison of Baseline Corrected DT6 in the Transverse Direction during Biaxial 1

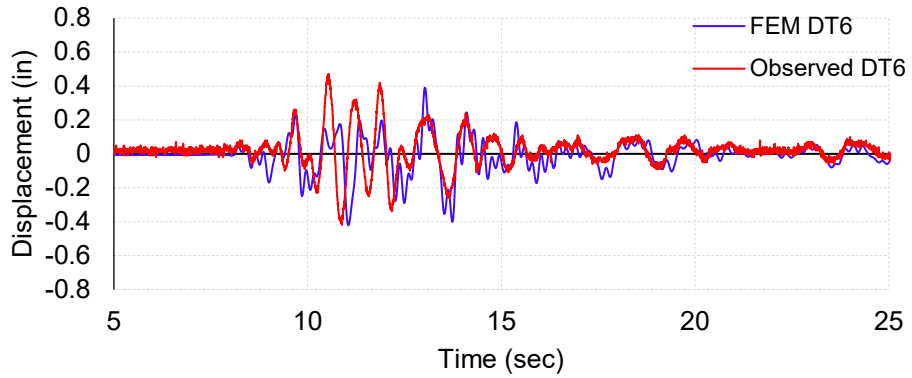

Figure 19. Displacement TH Comparison of Baseline Corrected DT7 in the Transverse Direction during Biaxial 1

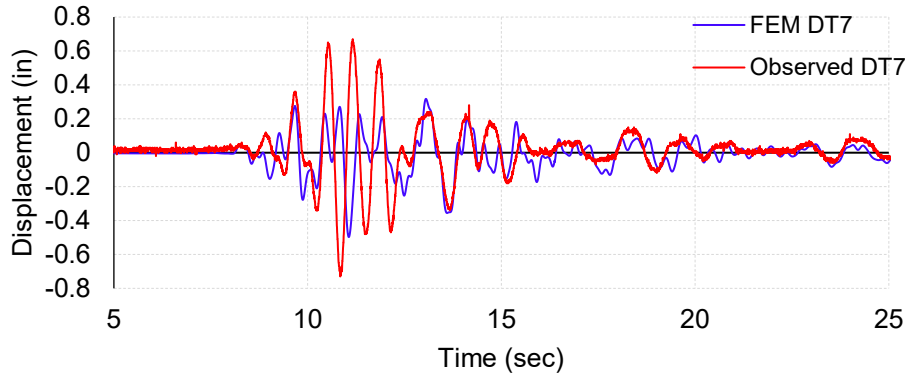

Figure 20. Displacement TH Comparison of Baseline Corrected DT6 in the Transverse Direction during Biaxial 2

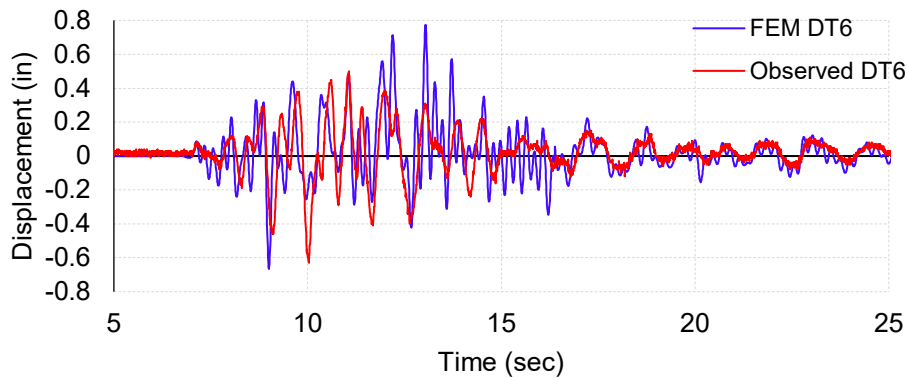

Figure 21. Displacement TH Comparison of Baseline Corrected DT7 in the Transverse Direction during Biaxial 2

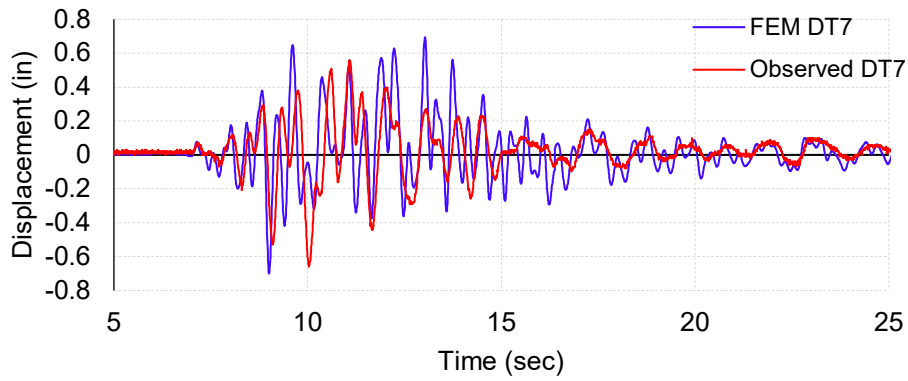

The acceleration data from the FEM were also compared with the observed data of the bridge to check the goodness of fit of the updated finite element model. Figures 22 to 25 show the comparison between absolute acceleration in the FEM and that of the observed bridge response.

Figure 22. Acceleration TH Comparison of AT2 in the Transverse Direction during Biaxial 1

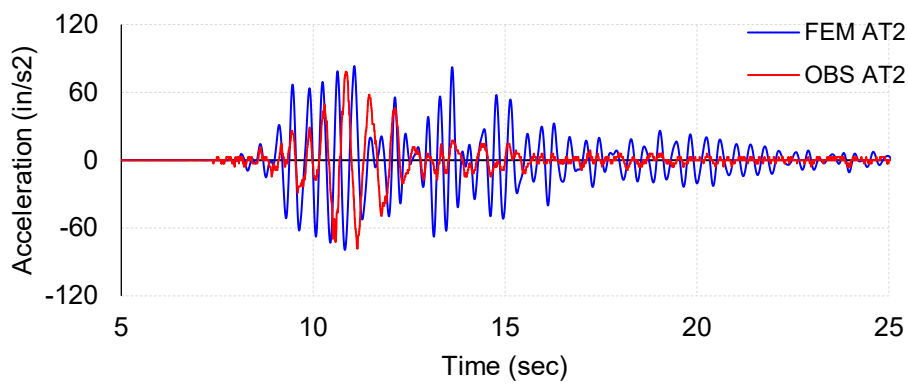

Figure 23. Acceleration TH Comparison of AT3 in the Transverse Direction during Biaxial 1

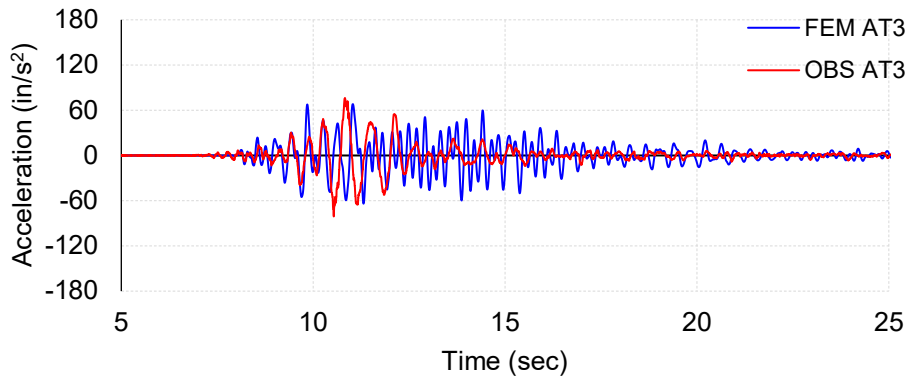

Figure 24. Acceleration TH Comparison of AT2 in the Transverse Direction during Biaxial 2

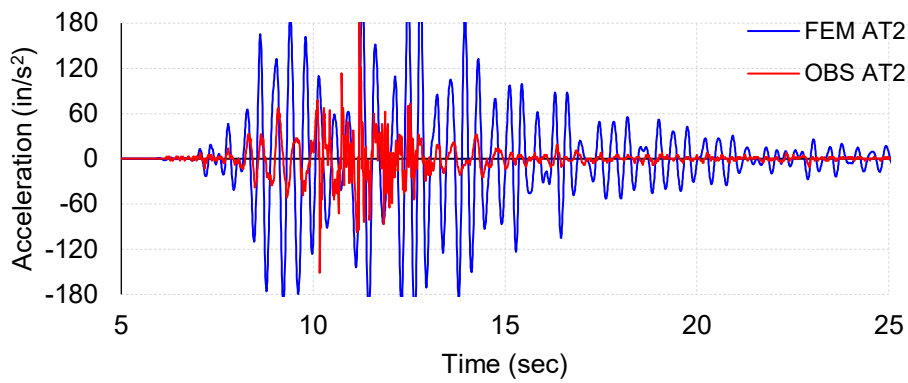

Figure 25. Acceleration TH Comparison of AT3 in the Transverse Direction during Biaxial 2

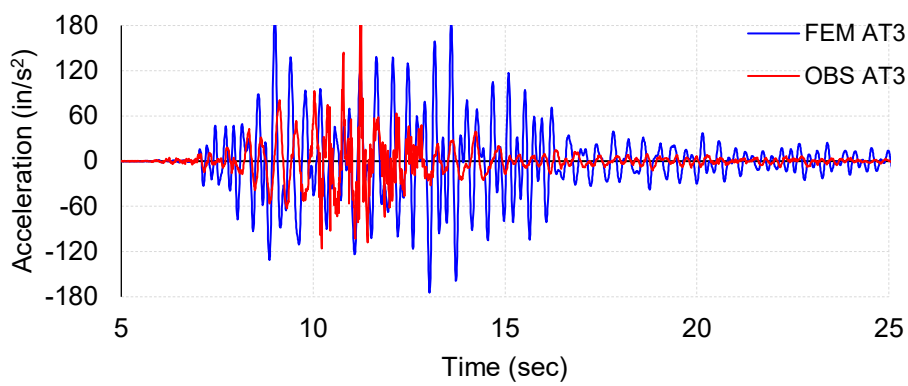

The plots of the displacement time history and acceleration time history reveal that the response of the FEM reasonably matches with the recorded response of the actual bridge. Thus, the goodness of agreement is such that the finite element model resembles the original bridge model. The FEM is then utilized to better understand the behavior of the actual bridge and its frequency

responses during various biaxial motions. The FEM also will help us to better investigate the wave propagation in the bridge and our wave method for identification of it.

Modal Frequencies and Mode Shapes Comparison

Table 2 shows the modal characteristics of the updated FE model with observed characteristics during Biaxial 2 input motion. The following factors contribute to achieving the desired modal response of the bridge: compressive strength of the concrete, correct geometry and cracked flexural stiffness of the bent cap, abutments, columns and deck, weight and location of dead load, and blocks and leads on the bridge. The deck of the bridge remained elastic throughout all the seven biaxial damaging events. The overall bridge response stayed elastic during the first three biaxial tests and then it started to sustain damage in the columns slowly during the last four biaxial tests.

Table 2. Comparison of Modal Characteristics of Updated FEM with Observed Characteristics

	Transverse Direction			
Resorted Mode #	Global Mode #	Apparent Frequencies $f_{i,\text{app}}$ (Hz)	FEM f_i (Hz)	$\Delta f_i / f_{i,\text{app}}$
1	1	2.777	2.61	6.01%
2	3	N/A*	3.21	N/A*
3	6	N/A*	4.59	N/A*

* The mode is not readable.

The shapes of the first and second modes in the transverse direction and the first mode in the vertical and longitudinal directions are shown for reference. Figures 26 to 28 show the shapes of the modes in different directions.

Figure 26 (two pages). First and Second Mode of the Bridge in the Transverse Direction

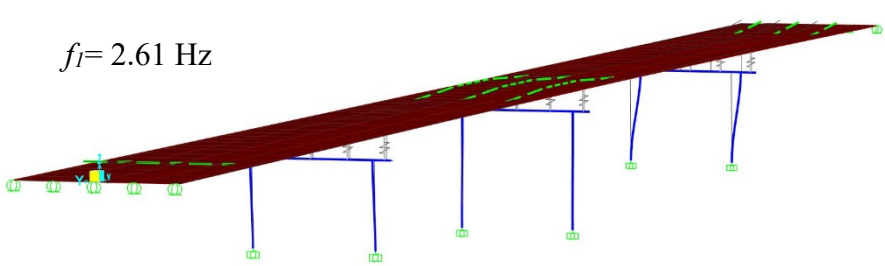

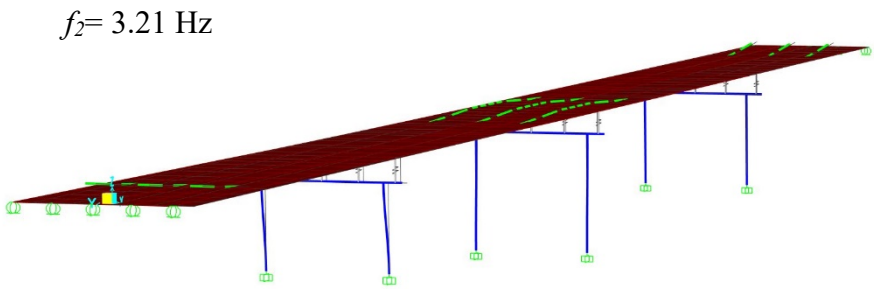

Figure 27. First Mode of the Bridge in the Vertical Direction

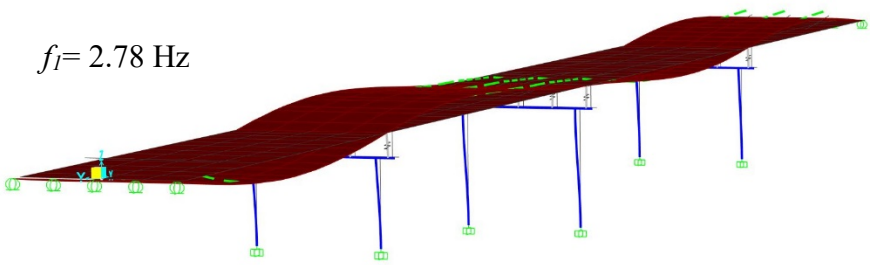

Figure 28. First Mode of the Bridge in the Longitudinal Direction

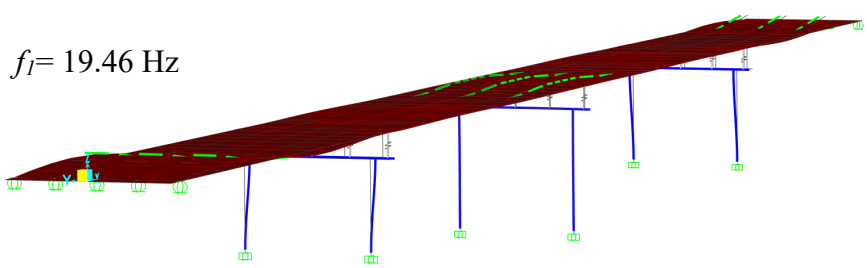

To further understand the dynamic response of our finite element model and that of the actual bridge, a detailed comparison was also made between the transfer functions (TF) for the Biaxial 1 and Biaxial 2 motions. The comparison was made for the pair of sensors AT3 – ST3, as shown in Figure 29. Both responses' first mode of vibration coincide reasonably at about 2.5 Hz.

Figure 29. Comparing TF of Observed Response with FEM Response for AT3 – ST3 during Biaxial 1 and Biaxial 2

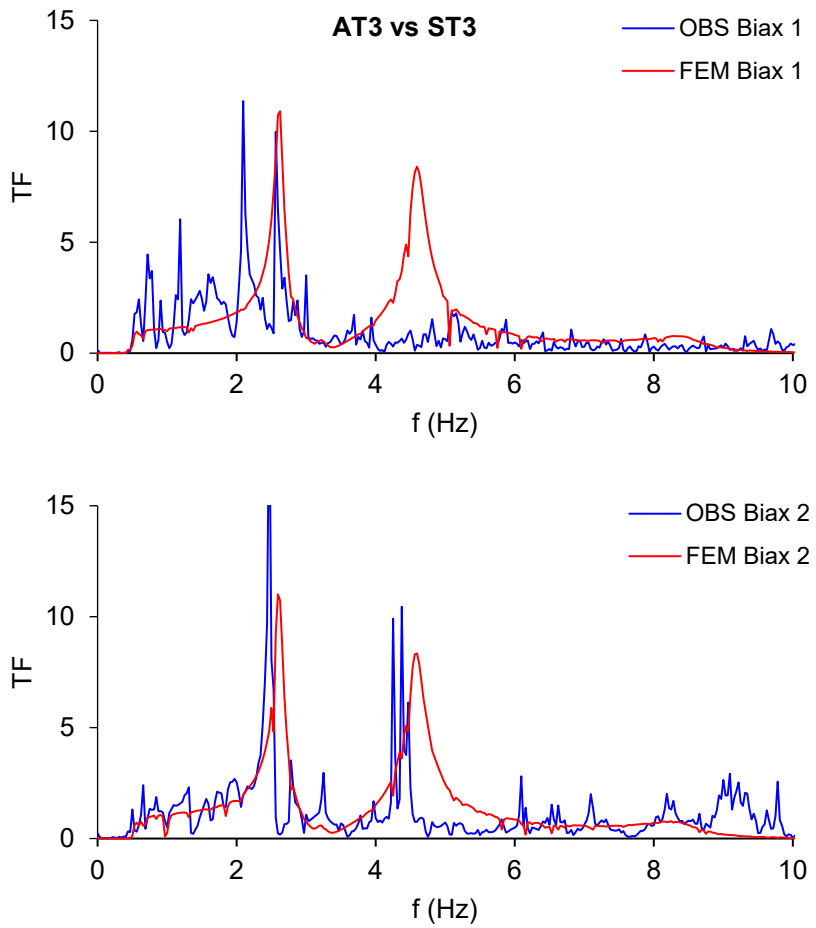

A Comparison of Calculated Impulse Response Functions: Actual Bridge versus FEM

A comparison was drawn between the IRFs of the pair AT3 – ST3 for Biaxial 1 and Biaxial 2, mainly to investigate whether the IRF of the FEM of the bridge resembled the IRF from the observed response (i.e., actual bridge). Figure 30 shows the comparison for the pair AT3 – ST3.

Figure 30. Comparing Raw IRF of Observed Response with FEM Response of AT3 – ST3 during Biaxial 1 and Biaxial 2

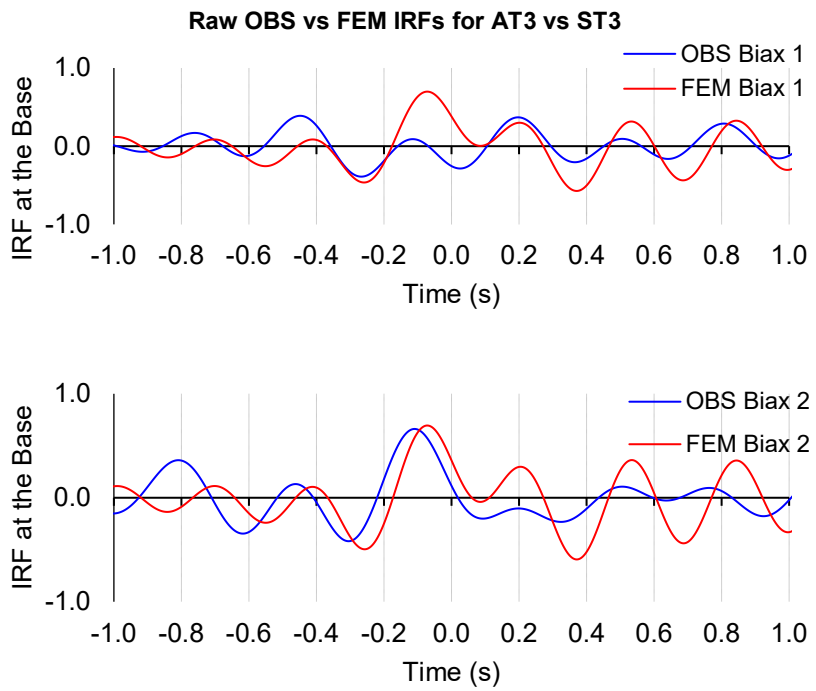

Summary and Discussion

Comparing displacement time history and acceleration time history responses at the deck level shows that there is reasonable agreement between the finite element model and the actual bridge's response. There are minor differences between the actual bridge and our model's response caused primarily by modeling assumptions (such as the exact location of lead blocks; cracked section properties of bent cap, column, and deck; and exact path of tendons along the middle two spans). Nonetheless, the FEM response agrees with the recorded response reasonably well. The modal frequency of the finite element model was very close to the recorded modal response in the transverse direction. The FEM model is then utilized to better understand the behavior of the actual bridge and its frequency responses during various biaxial motions, as discussed in Chapter IV.

IV. Wave Method Identification of the Bridge

4.1 Input Excitations of the Bridge

This chapter presents the selection and filtering of the input motions which were used as the signal in our receiving station within our wave-based identification process. The tested bridge experienced a series of excitations which progressively increased in amplitude. These excitations include seven biaxial motions which were utilized in this report.

The acceleration, displacement, and velocity of the bridge were recorded during the seven biaxial excitations recorded. Every time the bridge was tested, the biaxial input excitations increased in amplitude (i.e., acceleration) to further damage the bridge. Table 3 shows a summary of the shake-table accelerations for the seven biaxial tests. Then, Figure 31 presents the raw shake-table displacement time history in the transverse direction, which shows that the motion amplitudes increase in magnitude from Biaxial 1 to Biaxial 7. It is noteworthy that the input accelerations for Biaxial 6 and Biaxial 7 were identical.

Table 3. Shake-Table Accelerations Summary for the Seven Biaxial Tests*

Test No.	Test Date	Test Type	Target Motion PGA (g)	
			Trans.	*Long.*
1D	Feb. 12, 2007	Biaxial	0.075	0.09
2	Feb. 12, 2007	Biaxial	0.15	0.18
3	Feb. 13, 2007	Biaxial	0.25	0.3
4D	Feb. 13, 2007	Biaxial	0.5	0.6
5	Feb. 15, 2007	Biaxial	0.75	0.9
6	Feb. 15, 2007	Biaxial	1	1.2
7	Feb. 15, 2007	Biaxial	1	1.2

* Adopted from Nelson et al. 2007

Figure 31. Ground Displacement Time History of Shake-Table 2 in the Transverse Direction (Generated using unfiltered ground acceleration time history)

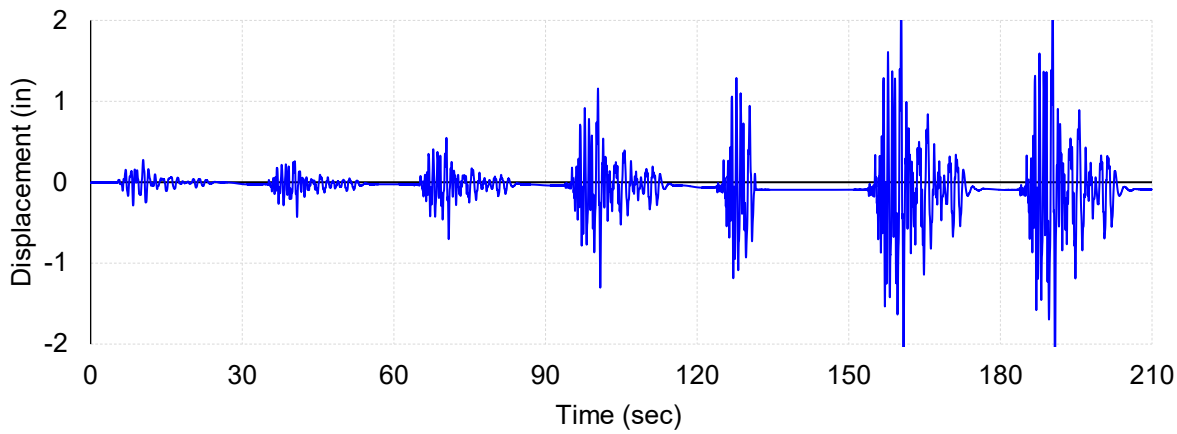

4.2 Introducing Two Scenarios for Wave Passage

This section presents two scenarios of wave passage in the bridge. Each scenario is used to obtain the impulse response function (IRF) and transfer functions (TFs) of the bridge along a specific wave path. The accelerometer channels located on the bridge deck and on the shake-tables were utilized according to these scenarios. The first scenario includes the wave passage through the columns only. Therefore, the sensors which are exactly on top of the bents and those at the base of them were used. The second scenario considers the wave passage through the columns and portion of the bridge deck. Hence, the sensors that are located at the mid-span of the bridge were used. Channels AT7, AT5, and AT3 are placed on top of Bents 1, 2, and 3, respectively, which are utilized in wave passage scenario I. The other channels, AT8, AT6, AT4, and AT2, are located at the mid length of each span, whereas AT9 and AT1 are located at the south and north abutments. These sensors are used in wave passage scenario II.

A MATLAB script was written to obtain the impulse response function and transfer function of the bridge. The wave propagates from the virtual source station (deck level) to the receiving stations (shake-table level). Figures 32 and 33 depict how the wave propagates in wave passage scenarios I and II, respectively.

Figure 32. Scenario I of Wave Passage where Propagation Occurs in Piers

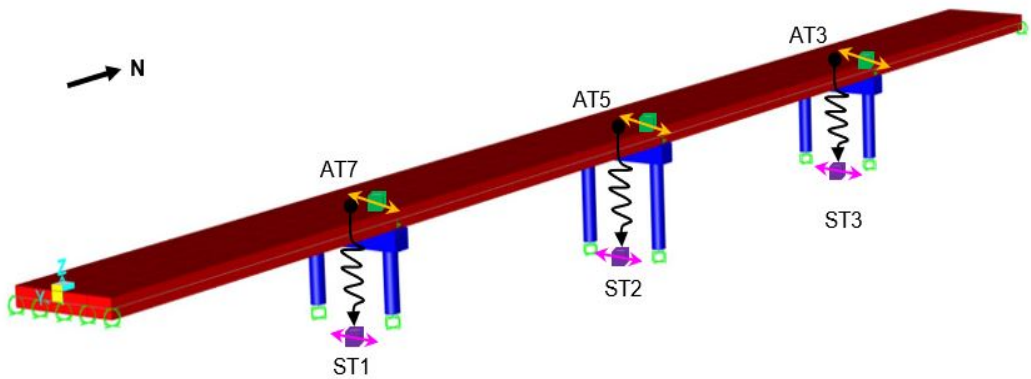

Figure 33. Wave Passage Scenario II where Propagation Occurs in Decks and Piers

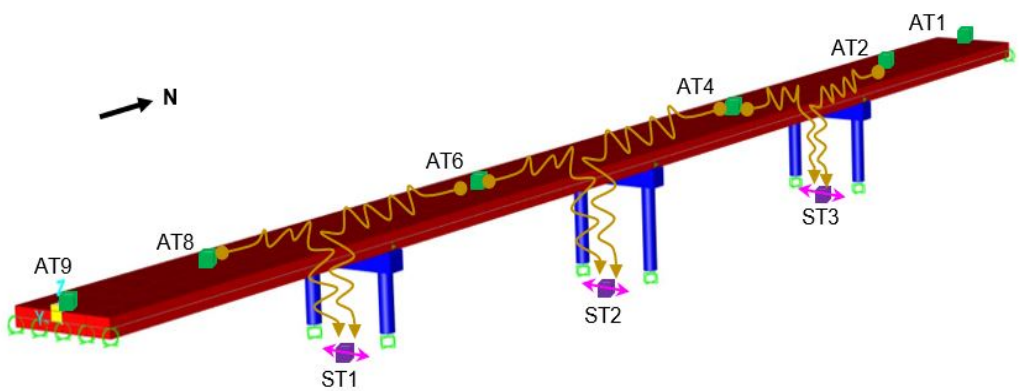

4.3 Uniform Shear Beam Model Fitted into Recorded Bridge Response During Seven Shakings

A uniform shear beam model is used to model the case study bridge between each pair of sensors, as shown in Figures 32 and 33. The IRFs and TFs of the bridge were computed at the boundaries between the layers using MATLAB. The recorded acceleration response provides the observed IRFs and TFs of the bridge. This chapter discusses in detail the fitting of the shear beam model's IRF into the IRF computed from the recorded bridge response. In addition, there is a sensitivity analysis of the effects of damping ratio and fitting frequency band on the identification results. Comparisons of the estimated shear wave velocities, estimated percentage of change in velocities, and the root mean square error of the fits are discussed for each pair of sensors under each scenario.

An Analysis of the Effect of Frequency Bands on the Observed IRFs and the Fitting Results

A detailed analysis was carried out for wave passage scenarios I and II to fit the shear beam model to the observed bridge response. IRFs of the shear beam were obtained from inverse Fourier transform of the lowpass filtered transfer functions of the beam. The width of the IRF pulse at the

source (i.e., deck), and consequently the width of the acausal and causal pulses at the receiving station (i.e., base), is a function of the chosen cut-off frequency (i.e., bandwidth). Initially, for wave passage scenarios I and II, the authors tried different frequency bands for the pairs AT3 – ST3 and AT6 – ST2 to achieve the best fit into the IRF of recorded data. The authors chose the cutoff frequency such that the frequency passband included the first vibrational mode of the bridge. In the time domain, the IRFs were fitted only around the time windows in which the main acausal and causal pulses occurred. The shear wave velocity (c), percentage of change in velocity ($\Delta c/c$), and normalized root mean square errors are plotted for different frequency bands to reveal the trends for the seven biaxial motions. Figure 34 and Table 4 show the results of varying frequency bands for the AT3 – ST3 comparisons. The shear beam model's damping was assumed to be 5% for these identifications.

Figure 34. Comparison between Estimated Shear Wave Velocity, Percentage Change in Velocity, and Normalized Root Mean Square Error (respectively) having Different Frequency Bands for AT3 – ST3

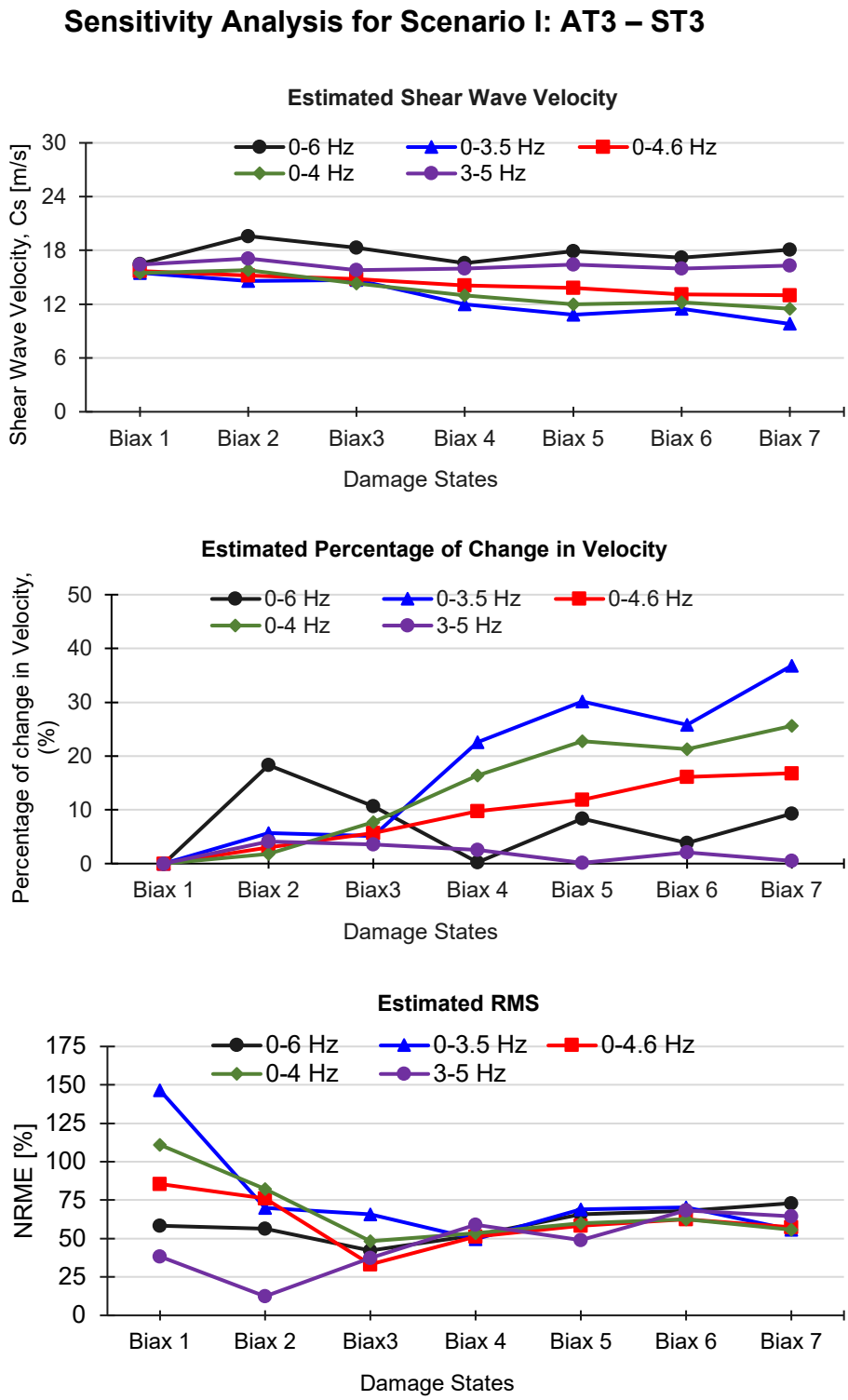

Table 4 (two pages). Identification Results for a Uniform Shear Beam Model Fitted into the Observed Bridge Transverse Response with Different Frequency Bands for AT3 – ST3

	Fitted Shear Beam into Bridge Transverse Response (Band-pass filtered **0–3.5** Hz)				Fitted Shear Beam into Bridge Transverse Response (Band-pass filtered **0–4** Hz)			
Event	c [m/s]	σ_c [m/s]	NRMSE %	$\Delta c/c$ %	c [m/s]	σ_c [m/s]	NRMSE %	$\Delta c/c$ %
Biaxial 1	15.5	0.5	146.4	0.0	15.5	0.5	111.0	0.0
Biaxial 2	14.6	0.6	98.8	5.7	15.8	0.7	82.1	1.8
Biaxial 3	14.7	0.4	65.9	5.1	14.3	0.4	48.3	7.7
Biaxial 4	12.0	0.4	49.6	22.6	13.0	0.7	53.4	16.4
Biaxial 5	10.8	0.5	69.1	30.1	12.0	0.5	59.9	22.8
Biaxial 6	11.5	1.1	70.4	25.8	12.2	1.0	62.7	21.3
Biaxial 7	9.8	0.4	55.9	36.8	11.5	0.6	55.7	25.6

	Fitted Shear Beam into Bridge Transverse Response (Band-pass filtered **0–4.6** Hz)				Fitted Shear Beam into Bridge Transverse Response (Band-pass filtered **0–6** Hz)			
Event	c [m/s]	σ_c [m/s]	NRMSE %	$\Delta c/c$ %	c [m/s]	σ_c [m/s]	NRMSE %	$\Delta c/c$ %
Biaxial 1	15.7	0.5	85.5	0	16.4	1.1	38.4	0.0
Biaxial 2	15.2	0.7	76.0	3.0	17.1	0.3	12.4	-4.1
Biaxial 3	14.8	0.3	33.2	5.7	15.8	1.2	37.5	3.6
Biaxial 4	14.1	0.7	51.2	9.7	16.0	3.3	59.1	2.5
Biaxial 5	13.8	0.7	58.2	11.9	16.4	2.4	49.0	0.1
Biaxial 6	13.1	0.9	62.6	16.1	16.0	4.9	68.3	2.1
Biaxial 7	13.0	0.7	57.5	16.8	16.3	4.5	64.4	0.5

	Fitted Shear Beam into Bridge Transverse Response (Band-pass filtered **3–5** Hz)			
Event	c [m/s]	σ_c [m/s]	NRMSE %	$\Delta c/c$ %
Biaxial 1	15.5	0.5	111.0	0
Biaxial 2	15.8	0.7	82.1	1.8
Biaxial 3	14.3	0.4	48.3	7.7
Biaxial 4	13.0	0.7	53.4	16.4
Biaxial 5	12.0	0.5	59.9	22.8
Biaxial 6	12.2	1.0	62.7	21.3
Biaxial 7	11.5	0.6	55.7	25.6

Sensitivity analyses of different frequency bands were also performed for wave passage scenario II, which involves sensor pair AT6 – ST2. Figure 35 and Table 5 present a comparison of identification results for all seven biaxial motions and for varying frequencies.

Figure 35. Comparison between Estimated Shear Wave Velocity, Percentage Change in Velocity, and Normalized Root Mean Square Error (respectively) having Different Frequency Bands for AT6 – ST2

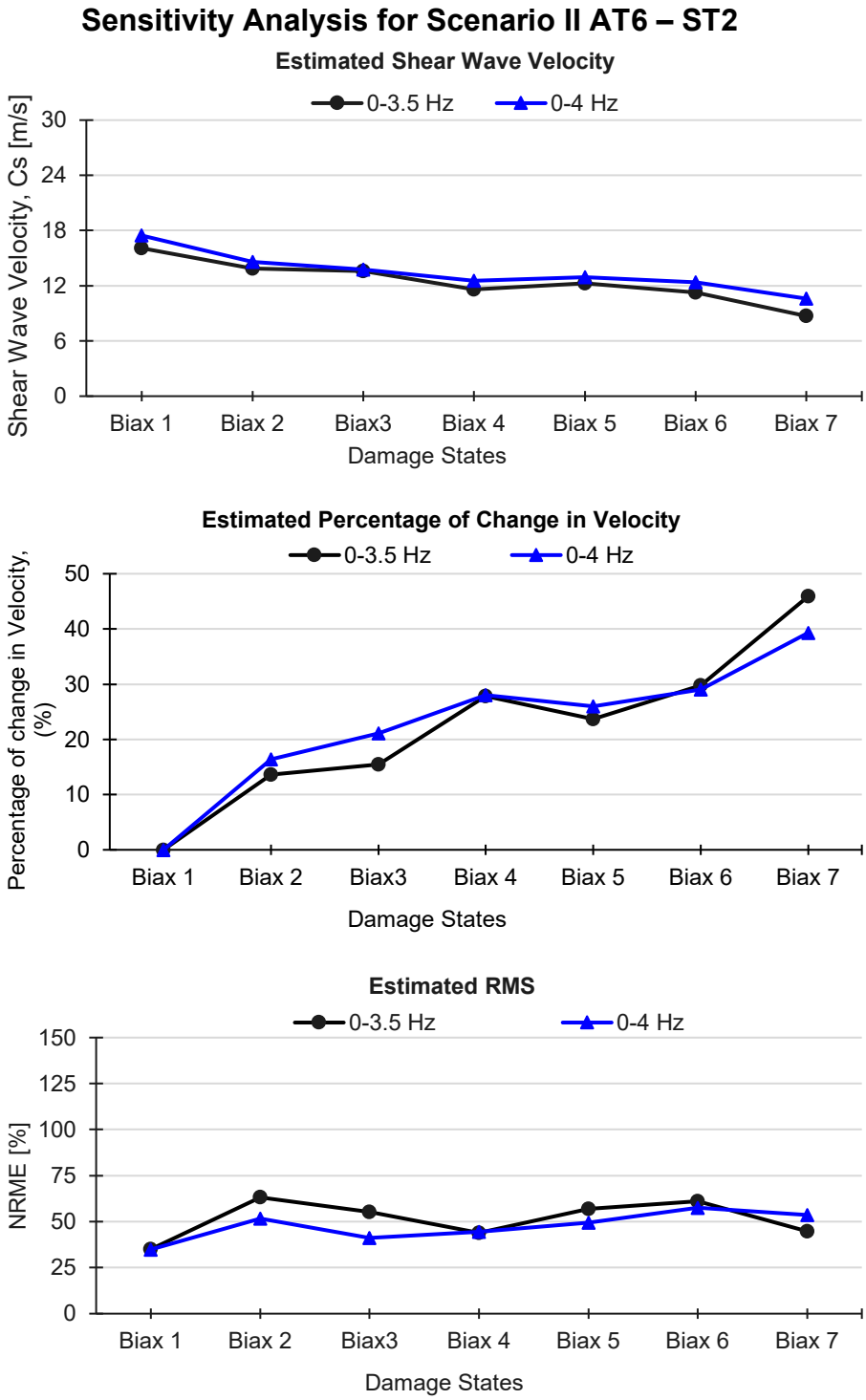

Table 5. Identification Results for a Uniform Shear Beam Model Fitted into the Observed Bridge Transverse Response with Different Frequency Bands for AT6 – ST2

	Fitted Shear Beam into Bridge Transverse Response (Band-pass filtered **0–3.5** Hz)				Fitted Shear Beam into Bridge Transverse Response (Band-pass filtered **0–4** Hz)			
Event	c [m/s]	σ_c [m/s]	NRMSE %	$\Delta c/c$ %	c [m/s]	σ_c [m/s]	NRMSE %	$\Delta c/c$ %
Biaxial 1	16.1	0.1	35.0	0.0	17.5	0.2	34.9	0.0
Biaxial 2	13.9	0.5	63.2	13.6	14.6	0.5	51.7	16.4
Biaxial 3	13.6	0.4	55.4	15.5	13.8	0.4	41.1	21.1
Biaxial 4	11.6	0.4	43.8	27.8	12.6	0.5	44.5	28.0
Biaxial 5	12.3	0.5	56.9	23.7	12.9	0.5	49.4	26.0
Biaxial 6	11.3	0.5	61.2	29.8	12.4	0.6	57.6	29.0
Biaxial 7	8.7	0.1	44.7	45.9	10.6	0.3	53.7	39.3

Effect of Damping as a Part of Sensitivity Analysis on the Identification Results

The shear beam model's damping affects the shape of the main pulses in the analytical IRFs. Hence, it can affect the goodness of the IRF fits. In this study, different damping ratios were used to fit the shear beam model into the observed bridge response to identify which damping gives the best fits for the IRFs. The best fits are defined according to the normalized mean square error as well as a visual inspection of the fitted IRFs to ensure the main pulses are fitted. In addition, trends in the identified shear wave velocities were assessed to identify outliers and extreme changes in the velocities for each of the damping ratios. For this sensitivity analysis, the channel pairs AT3 – ST3 (wave passage scenario I) and AT6 – ST2 (wave passage scenario II) were used. The identifications were performed for 1%, 5%, and 10% damping ratios and for biaxial motions 1, 3, and 6. Figure 36 shows the results of the IRFs' fits for varying damping ratios.

Figure 36. Comparison between Observed and Shear Beam Fitting with Different Damping for AT3 – ST3 during Biaxial 1, 3, and 6

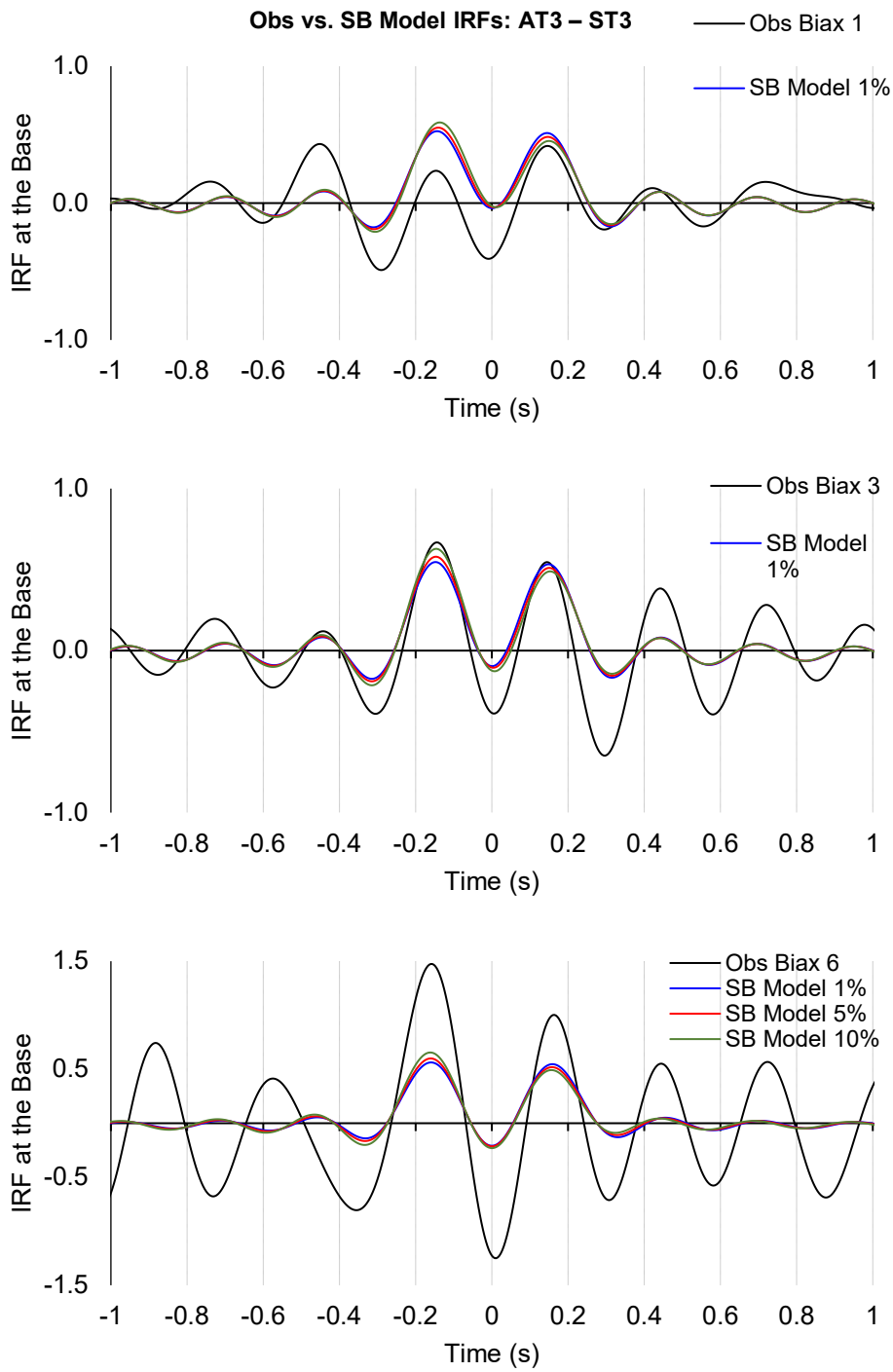

A similar comparison was performed for the pair AT6 – ST2 for wave passage scenario II for varying damping ratios. Figure 37 shows the plots of fitting shear beam (SB) to the observed response for varying damping ratios.

Figure 37. Comparison between Observed and Shear Beam Fitting with Different Damping for AT6 – ST2 during Biaxial 1, 3, and 6

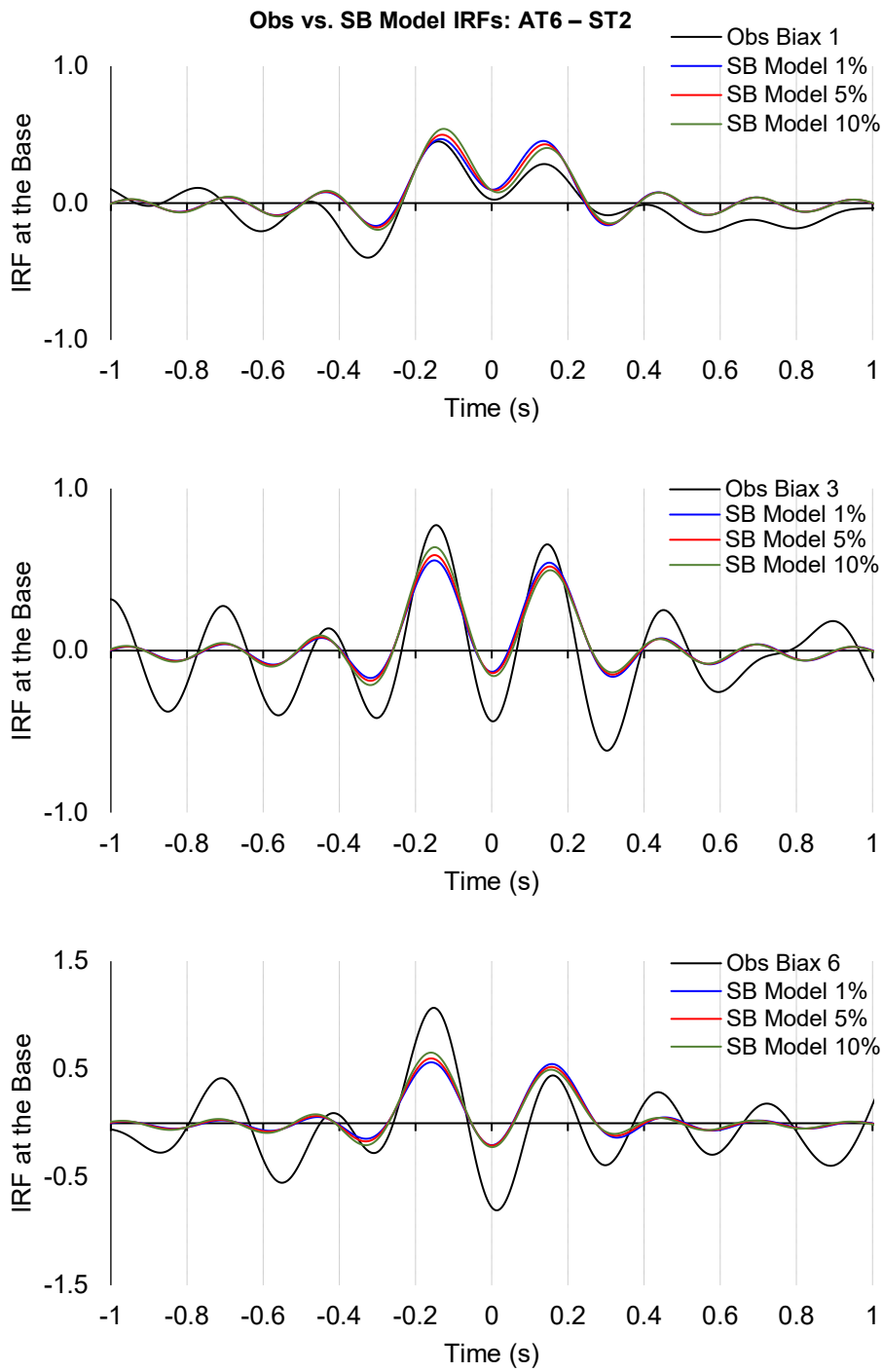

The sensitivity analysis for the damping ratios of the shear beam model revealed that there was a negligible effect on the shape of the main IRF pulses. Thus, there was a negligible effect on the estimated shear wave velocities. Also, it was noticed that damping affects the amplitude of the pulse by reducing the causal pulse's amplitude and increasing the acausal pulse's amplitude slightly.

Figure 38 shows a comparison of shear wave velocities, percentage of change in velocities, and normalized root mean square error. Table 6 also presents the results for the estimated shear wave velocities for varying damping ratios.

Figure 39 and Table 7 show similar sensitivity analyses on damping for one of the pairs of wave passage scenario II. A similar conclusion was drawn from these results as discussed above. In conclusion, the authors chose to use a constant damping ratio of 5% in the shear beam for all identification analyses.

Figure 38. Comparison between Estimated Shear Wave Velocity, Percentage Change in Velocity, and Normalized Root Mean Square Error (respectively) having 0–4 Hz Frequency Bandpass with Various Damping for AT3 – ST3

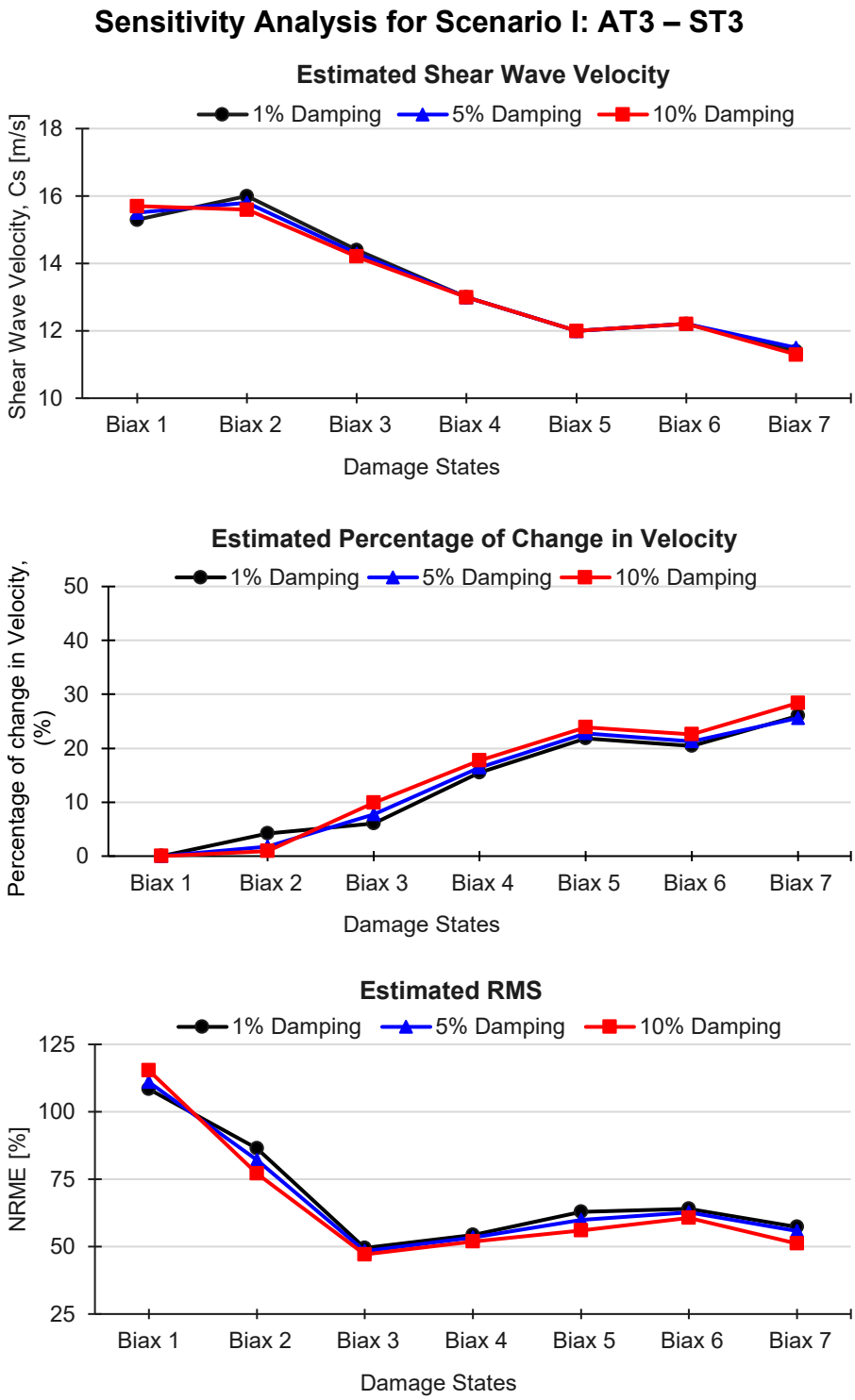

Table 6. Identification Results for a Uniform Shear Beam Model Fitted into the Observed Bridge Transverse Response with 1%, 5%, and 10% Damping for AT3 – ST3

	Fitted Shear Beam into Bridge Transverse Response (Band-pass filtered **0–4** Hz_1% damp.)				Fitted Shear Beam into Bridge Transverse Response (Band-pass filtered **0–4** Hz_5% damp.)			
Event	c [m/s]	σ_c [m/s]	NRMSE %	$\Delta c/c$ %	c [m/s]	σ_c [m/s]	NRMSE %	$\Delta c/c$ %
Biaxial 1	15.3	0.5	108.4	0.0	15.5	0.5	111.0	0.0
Biaxial 2	16.0	0.8	86.4	4.2	15.8	0.7	82.1	1.8
Biaxial 3	14.4	0.5	49.5	6.1	14.3	0.4	48.3	7.7
Biaxial 4	13.0	0.7	54.3	15.5	13.0	0.7	53.4	16.4
Biaxial 5	12.0	0.6	62.9	21.8	12.0	0.5	59.9	22.8
Biaxial 6	12.2	1.0	64.0	20.4	12.2	1.0	62.7	21.3
Biaxial 7	11.4	0.6	57.2	26.0	11.5	0.6	55.7	25.6

	Fitted Shear Beam into Bridge Transverse Response (Band-pass filtered **0–4** Hz_10% damp.)			
Event	c [m/s]	σ_c [m/s]	NRMSE %	$\Delta c/c$ %
Biaxial 1	15.7	0.5	115.3	0.0
Biaxial 2	15.6	0.6	77.1	0.9
Biaxial 3	14.2	0.4	47.1	9.9
Biaxial 4	13.0	0.6	51.9	17.7
Biaxial 5	12.0	0.4	55.9	23.9
Biaxial 6	12.2	0.8	60.7	22.6
Biaxial 7	11.3	0.4	51.2	28.4

Figure 39. Comparison between Estimated Shear Wave Velocity, Percentage Change in Velocity, and Normalized Root Mean Square Error (respectively) having Different Damping for AT6 – ST2

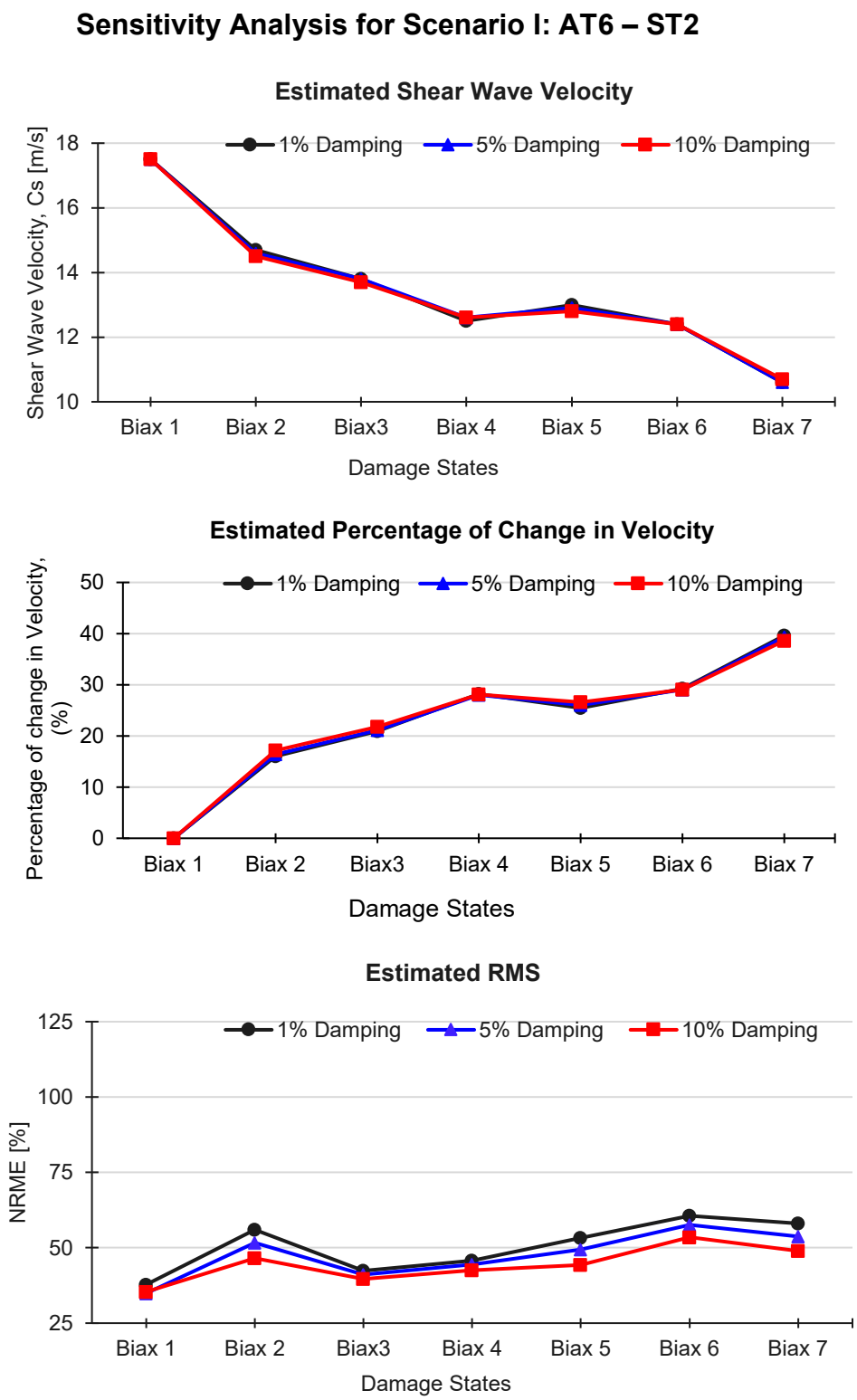

Table 7. Identification Results for a Uniform Shear Beam Model Fitted into the Observed Bridge Transverse Response with 1%, 5%, and 10% Damping for AT6 – ST2

	Fitted Shear Beam into Bridge Transverse Response (Band-pass filtered **0–4** Hz_1% damp.)				Fitted Shear Beam into Bridge Transverse Response (Band-pass filtered **0–4** Hz_5% damp.)			
Event	c [m/s]	σ_c [m/s]	NRMSE %	$\Delta c/c$ %	c [m/s]	σ_c [m/s]	NRMSE %	$\Delta c/c$ %
Biaxial 1	17.5	0.2	37.8	0.0	17.5	0.2	34.9	0.0
Biaxial 2	14.7	0.5	56.0	16.0	14.6	0.5	51.7	16.4
Biaxial 3	13.8	0.5	42.3	20.9	13.8	0.4	41.1	21.1
Biaxial 4	12.5	0.5	45.8	28.2	12.6	0.5	44.5	28.0
Biaxial 5	13.0	0.6	53.3	25.5	12.9	0.5	49.4	26.0
Biaxial 6	12.4	0.7	60.6	29.2	12.4	0.6	57.6	29.0
Biaxial 7	10.6	0.3	58.1	39.6	10.6	0.3	53.7	39.3

	Fitted Shear Beam into Bridge Transverse Response (Band-pass filtered **0–4** Hz_10% damp.)			
Event	c [m/s]	σ_c [m/s]	NRMSE %	$\Delta c/c$ %
Biaxial 1	17.5	0.2	35.4	0.0
Biaxial 2	14.5	0.4	46.5	17.2
Biaxial 3	13.7	0.4	39.6	21.8
Biaxial 4	12.6	0.4	42.6	28.1
Biaxial 5	12.8	0.4	44.3	26.6
Biaxial 6	12.4	0.5	53.5	29.0
Biaxial 7	10.7	0.2	49.0	38.6

Bridge Identification Results Through Fitting Shear Beam Models into the Recorded Data During Seven Shakings

Detailed IRF and TF analysis was done for each of the pairs in wave passage scenarios I and II for all seven biaxial input motions. The results from the sensitivity analysis of damping ratios and frequency bands were used to choose the optimum damping and frequency band for the analysis of all pairs. Damping of 5% and a frequency band of 0–3.5 Hz were chosen for fitting the shear beam model to the actual bridge's response. Figure 40 presents the fitted impulse response functions of the shear beam into that of actual bridge for biaxial motions 1, 4, and 7. The results are for scenario I. The fit of the causal and acausal pulses is good. The shear wave velocities for the identified beams were extracted after the best fits had been achieved. Figure 41 shows the equivalent transfer functions for the identified beam and the actual bridge. It can be seen that the agreement between the shear beam model and the tested bridge in the frequency domain is acceptable as well. The transfer function comparisons are an additional check to ensure the fundamental mode of vibrations occur within a small range of frequency.

Figure 40. IRF of Uniform Shear Beam Fitted Model into the Bridge Observed IRF having Frequency Band [0–3.5 Hz] and 5% Damping for AT5 – ST2 during Biaxial 1, Biaxial 4, and Biaxial 7

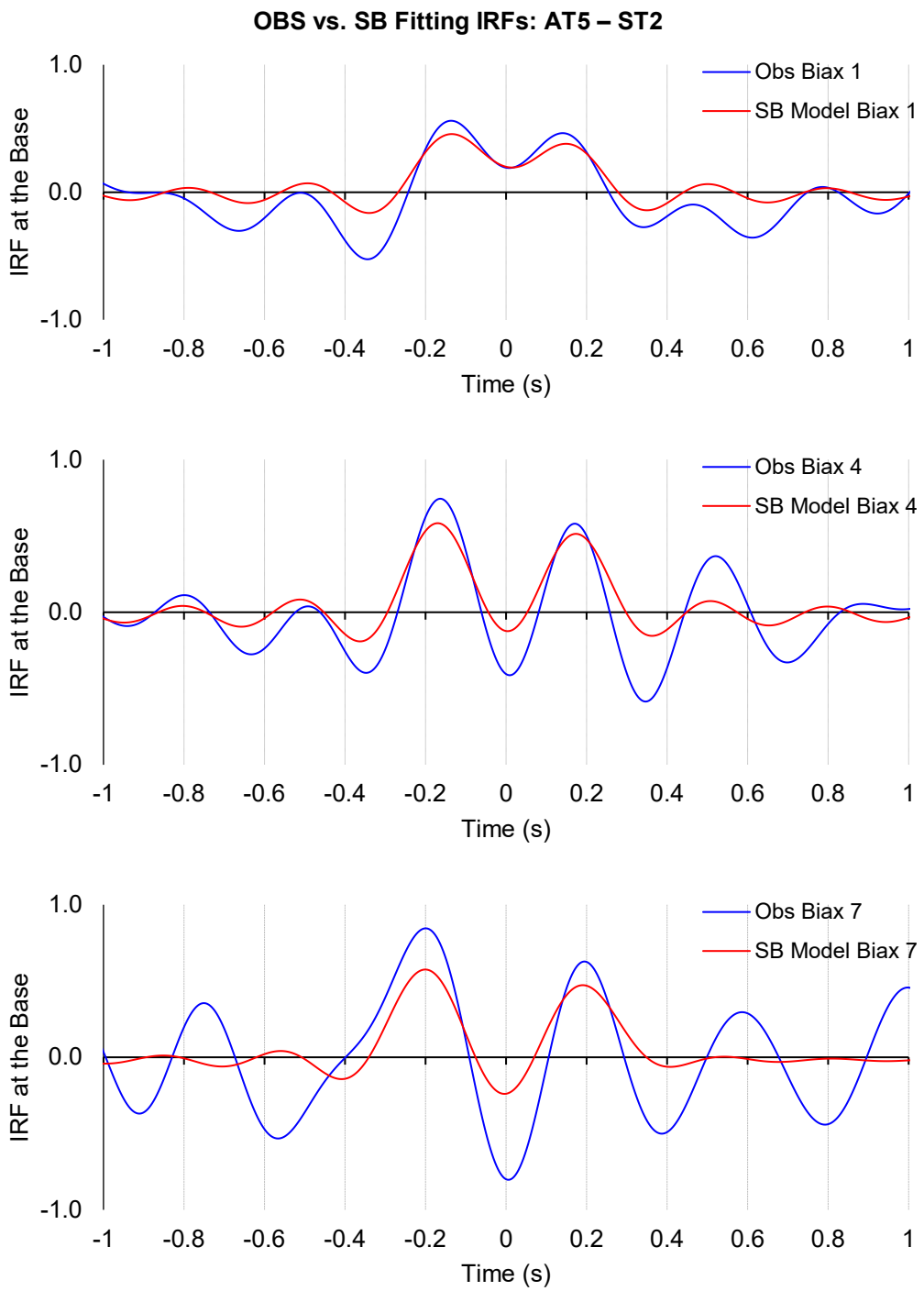

Figure 41. TF of Uniform Shear Beam Fitted Model into the Bridge Observed TF having Frequency Band [0–3.5 Hz] and 5% Damping for AT5 – ST2 during Biaxial 1, Biaxial 4, and Biaxial 7

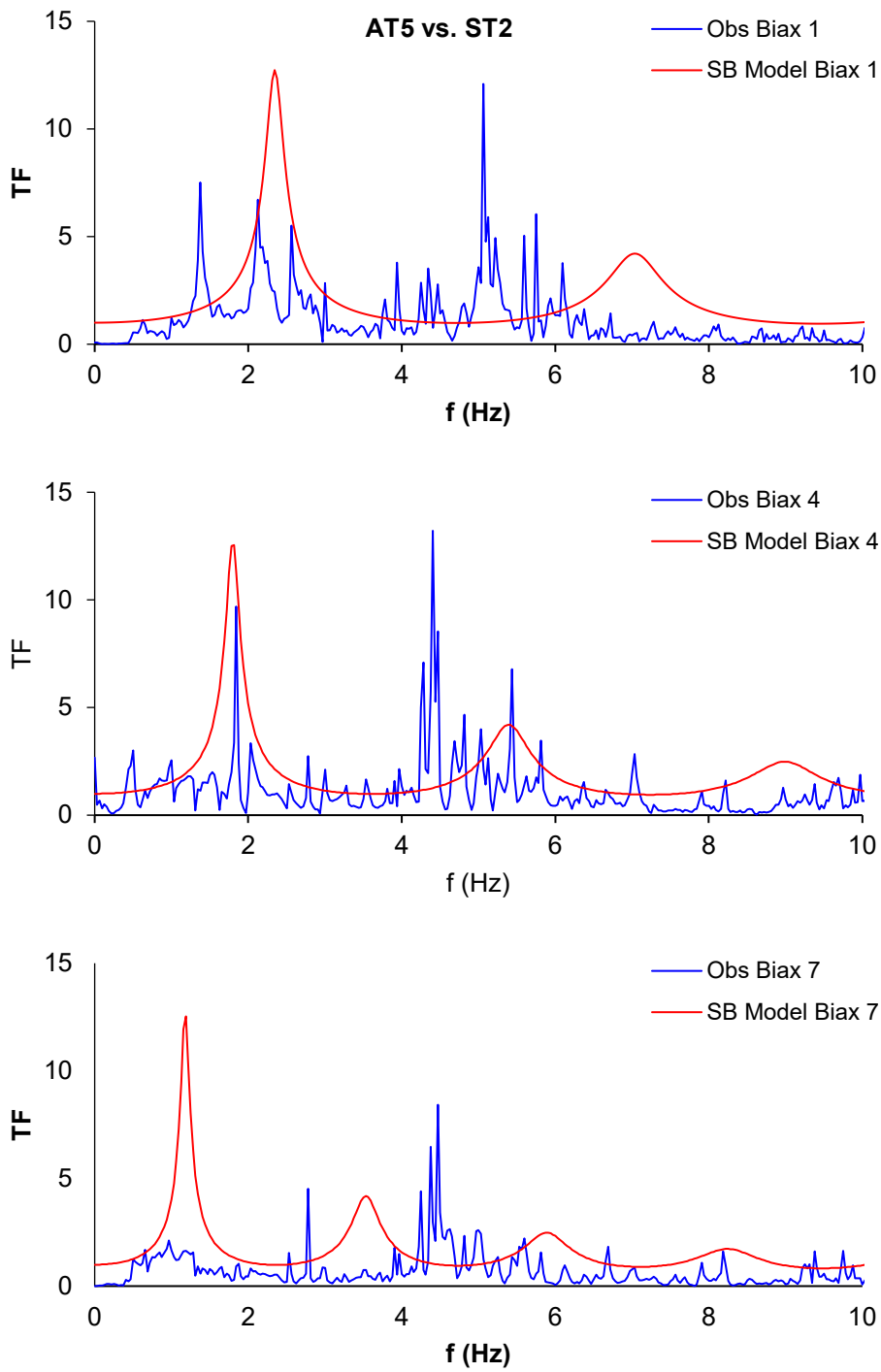

In summary, the comparison plots reveal that the identified shear beam model presents a reasonable agreement for both the IRFs and the TFs, and thus it can provide a good estimate of the actual bridge's stiffness along the wave path.

Furthermore, the authors compared similar plots for IRF and TF for wave passage scenario II. Figures 42 and 43 show these IRF and TF comparisons for Biaxial 1, Biaxial 4, and Biaxial 7. Figures 44, 45, and 46 present comprehensive comparison plots for the estimated shear wave velocities, percentage change in the velocities, and the fit's normalized root mean square error for the pairs of sensors next to Bent 1, Bent 2, and Bent 3, respectively.

Figure 42. IRF of Uniform Shear Beam Fitted Model into the Bridge Observed Response having Frequency Band [0–3.5 Hz] and 5% Damping for AT6 – ST2 during Biaxial 1, Biaxial 4, and Biaxial 7

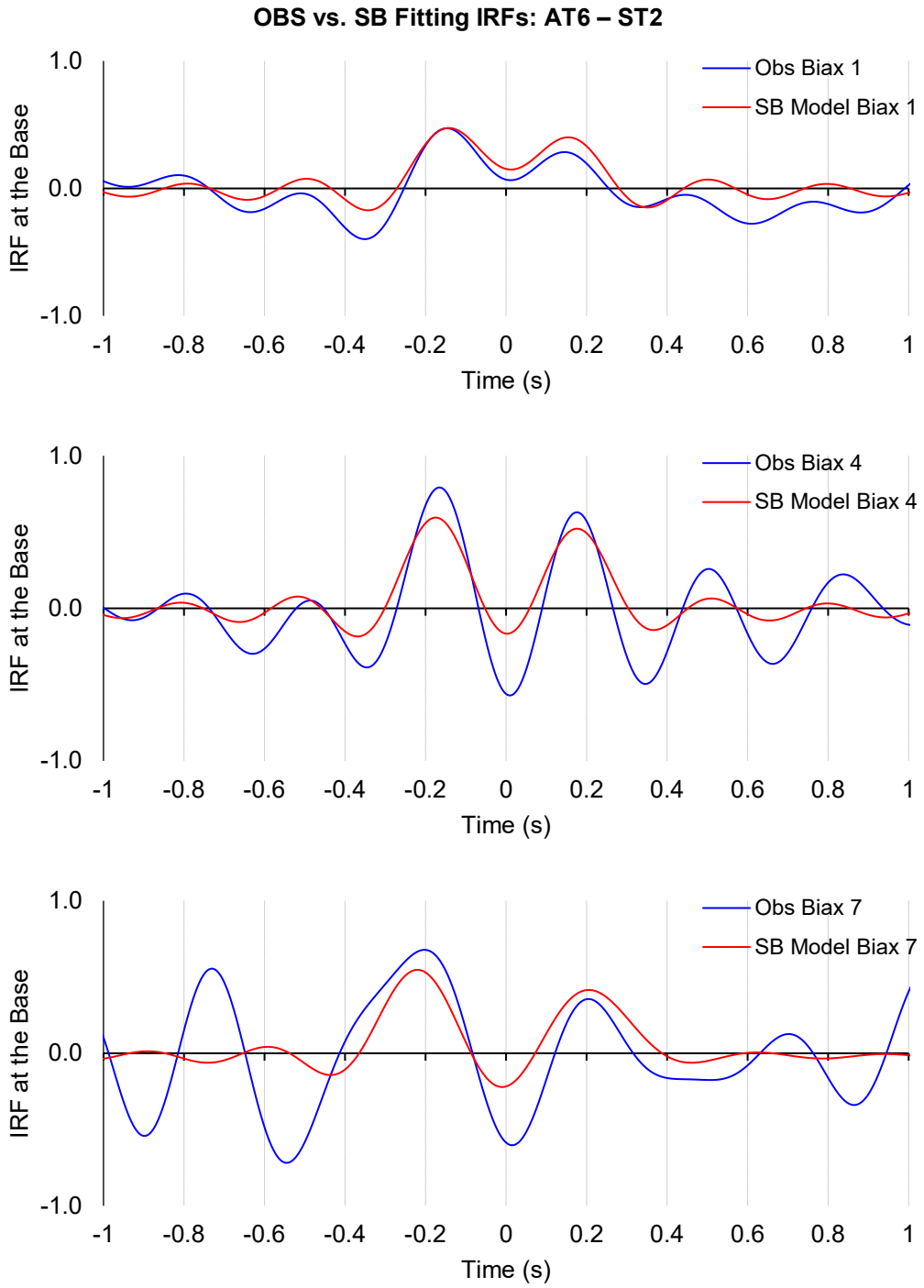

Figure 43. Transfer Function of Uniform Shear Beam Fitted Model into the Bridge Observed Response having Frequency Band [0–3.5 Hz] and 5% Damping for AT6 – ST2 during Biaxial 1, Biaxial 4, and Biaxial 7

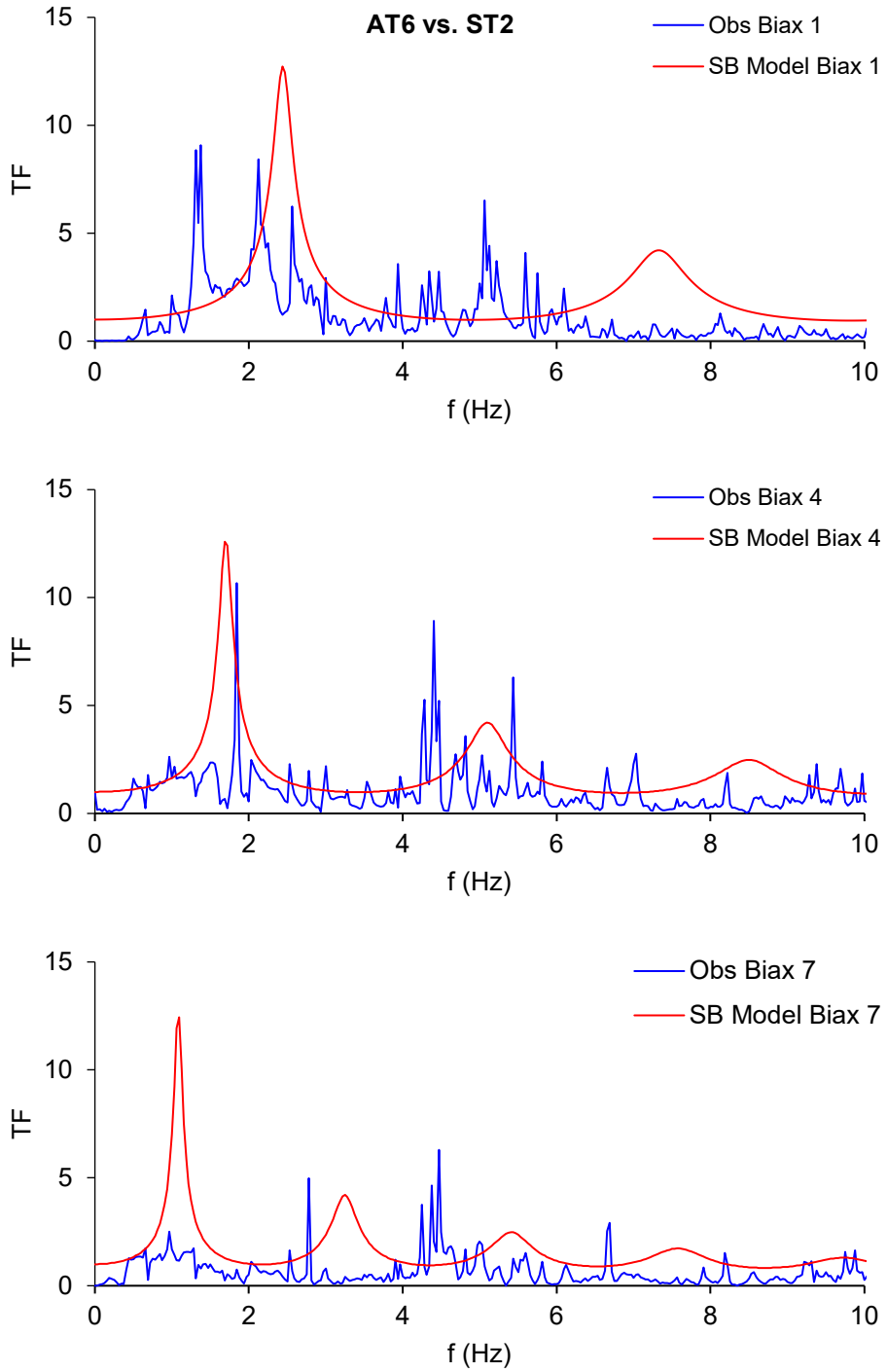

Figure 44. Comparison between Estimated Shear Wave Velocity, Percentage Change in Velocity, and Normalized Root Mean Square Error (respectively) for Pairs around Bent 1

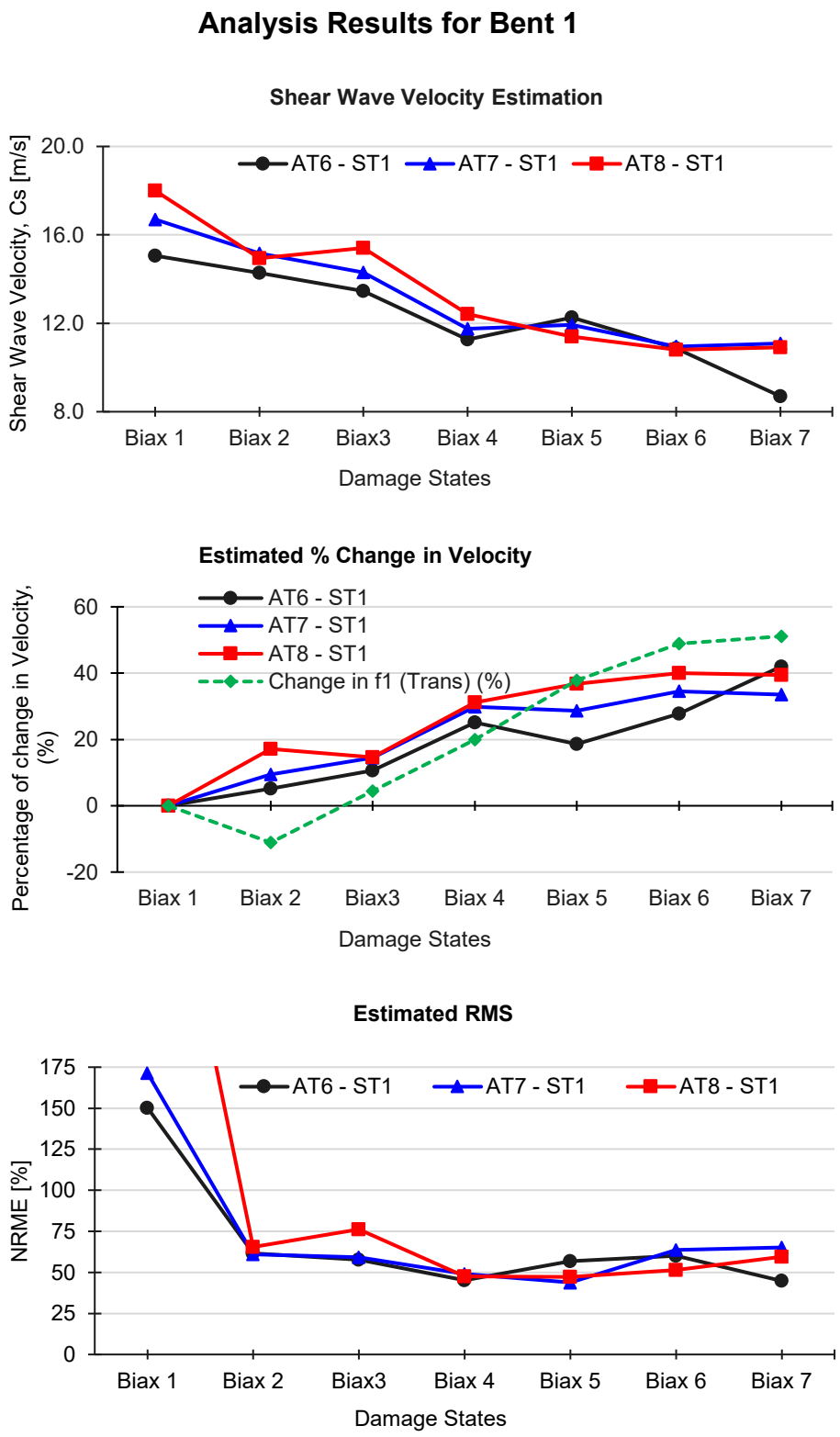

Figure 45. Comparison between Estimated Shear Wave Velocity, Percentage Change in Velocity, and Normalized Root Mean Square Error (respectively) for Pairs around Bent 2

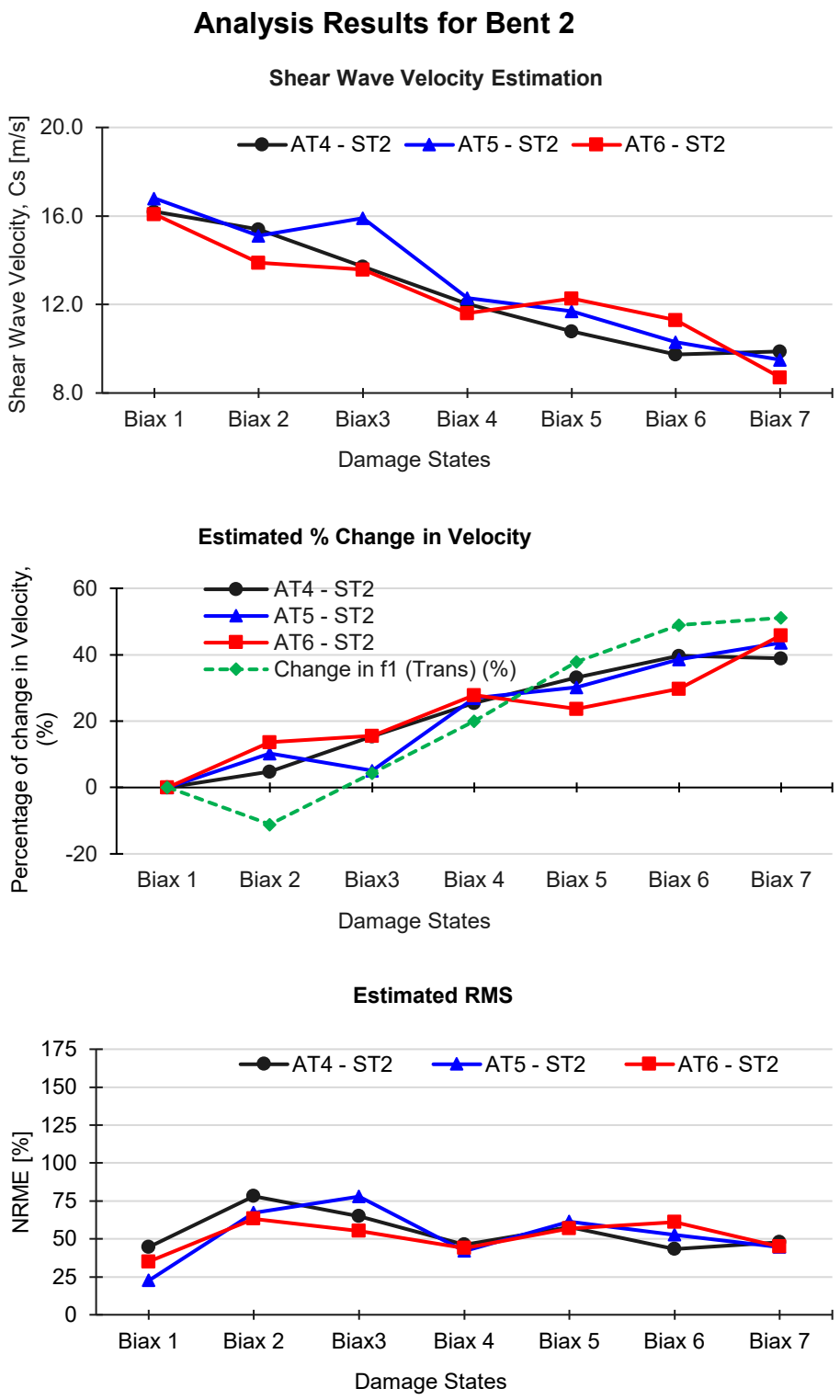

Figure 46. Comparison between Estimated Shear Wave Velocity, Percentage Change in Velocity, and Normalized Root Mean Square Error (respectively) for Pairs around Bent 3

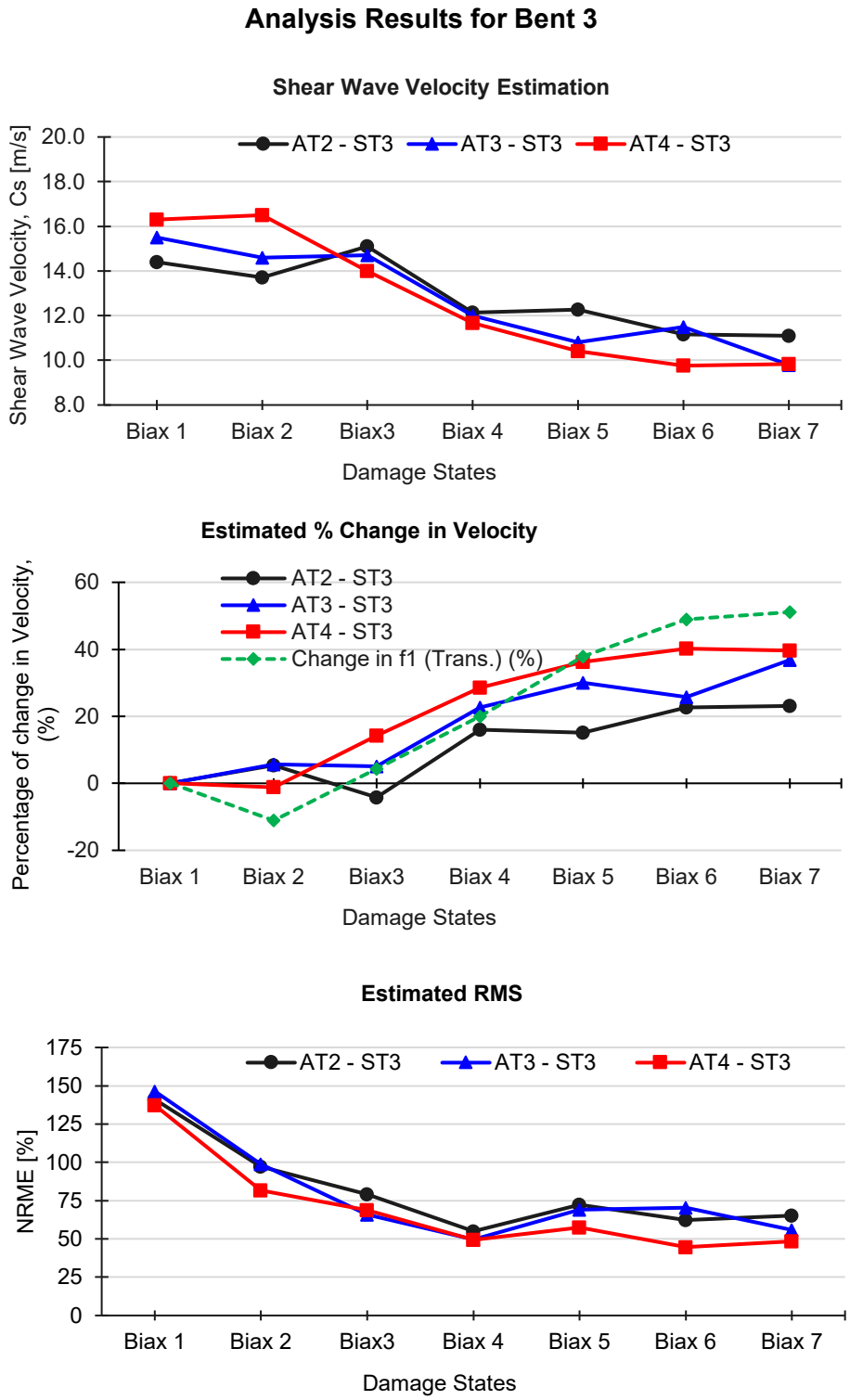

Table 8. Identification Results for a Uniform SB Model Fitted into the Observed Bridge Transverse Response with 5% Damping for AT3 – ST3

		Fitted Shear Beam into Bridge Transverse Response (Band-pass filtered **0–3.5** Hz)				
	Event	c [m/s]	σ_c [m/s]	$\frac{\sigma_c}{c}$ %	NRMSE %	$\Delta c/c$ %
AT3 – ST3	Biaxial 1	15.5	0.5	3.1	146.4	0.0
	Biaxial 2	14.6	0.6	4.4	98.8	5.7
	Biaxial 3	14.7	0.4	2.6	65.9	5.1
	Biaxial 4	12.0	0.4	3.3	49.6	22.6
	Biaxial 5	10.8	0.5	4.3	69.1	30.1
	Biaxial 6	11.5	1.1	9.7	70.4	25.8
	Biaxial 7	9.8	0.4	3.9	55.9	36.8

Table 9. Identification Results for a Uniform SB Model Fitted into the Observed Bridge Transverse Response with 5% Damping for AT3 – ST3

		Fitted Shear Beam into Bridge Transverse Response (Band-pass filtered **0–3.5** Hz)				
	Event	c [m/s]	σ_c [m/s]	$\frac{\sigma_c}{c}$ %	NRMSE %	$\Delta c/c$ %
AT5 – ST2	Biaxial 1	16.8	0.1	0.7	22.5	0.0
	Biaxial 2	15.1	0.5	3.2	67.2	10.2
	Biaxial 3	15.9	0.4	2.5	77.9	5.1
	Biaxial 4	12.3	0.3	2.8	41.9	27.0
	Biaxial 5	11.7	0.7	6.1	61.4	30.2
	Biaxial 6	10.3	0.3	3.4	52.6	38.6
	Biaxial 7	9.5	0.2	2.4	44.7	43.6

Table 10. Identification Results for a Uniform SB Model Fitted into the Observed Bridge Transverse Response with 5% Damping for AT7 – ST1

		Fitted Shear Beam into Bridge Transverse Response (Band-pass filtered **0–3.5** Hz)				
	Event	c [m/s]	σ_c [m/s]	$\frac{\sigma_c}{c}$ %	NRMSE %	$\Delta c/c$ %
AT7 – ST1	Biaxial 1	16.7	0.5	2.7	171.4	0.0
	Biaxial 2	15.2	0.4	2.4	60.9	9.4
	Biaxial 3	14.3	0.3	2.3	59.2	14.5
	Biaxial 4	11.7	0.4	3.3	49.0	29.8
	Biaxial 5	11.9	0.3	2.5	43.8	28.7
	Biaxial 6	10.9	0.8	7.1	63.8	34.5
	Biaxial 7	11.1	0.8	7.5	65.2	33.6

Table 11. Identification Results for a Uniform SB Model Fitted into the Observed Bridge Transverse Response with 5% Damping for AT2 – ST3

		Fitted Shear Beam into Bridge Transverse Response (Band-pass filtered **0–3.5** Hz)				
	Event	c [m/s]	σ_c [m/s]	$\frac{\sigma_c}{c}$ %	NRMSE %	$\Delta c/c$ %
AT2 – ST3	Biaxial 1	14.4	0.5	3.3	141.1	0.0
	Biaxial 2	13.7	0.6	4.5	97.2	5.4
	Biaxial 3	15.1	0.4	2.9	79.2	4.2
	Biaxial 4	12.1	0.4	3.2	55.0	16.0
	Biaxial 5	12.3	0.8	6.6	72.4	15.1
	Biaxial 6	11.2	0.8	7.1	62.3	22.7
	Biaxial 7	11.1	0.9	8.3	65.2	23.1

Table 12. Identification Results for a Uniform SB Model Fitted into the Observed Bridge Transverse Response with 5% Damping for AT4 – ST3

		Fitted Shear Beam into Bridge Transverse Response (Band-pass filtered **0–3.5** Hz)				
	Event	c [m/s]	σ_c [m/s]	$\frac{\sigma_c}{c}$ %	NRMSE %	$\Delta c/c$ %
AT4 – ST3	Biaxial 1	16.3	0.3	2.1	137.3	0.0
	Biaxial 2	16.5	0.5	3.2	81.8	-1.2
	Biaxial 3	14.0	0.5	3.4	68.8	14.3
	Biaxial 4	11.7	0.4	3.5	49.3	25.8
	Biaxial 5	10.4	0.3	2.5	57.4	31.7
	Biaxial 6	9.8	0.3	2.8	44.7	37.4
	Biaxial 7	9.8	0.3	3.2	48.4	36.8

Table 13. Identification Results for a Uniform SB Model Fitted into the Observed Bridge Transverse Response with 5% Damping for AT4 – ST2

		Fitted Shear Beam into Bridge Transverse Response (Band-pass filtered **0–3.5** Hz)				
	Event	c [m/s]	σ_c [m/s]	$\frac{\sigma_c}{c}$ %	NRMSE %	$\Delta c/c$ %
AT4 – ST2	Biaxial 1	16.2	0.2	1.0	44.5	0.0
	Biaxial 2	15.4	0.5	3.2	78.1	4.8
	Biaxial 3	13.7	0.5	3.4	64.8	15.4
	Biaxial 4	12.0	0.4	3.3	46.2	25.5
	Biaxial 5	10.8	0.3	2.6	57.7	33.2
	Biaxial 6	9.7	0.2	2.5	43.3	39.7
	Biaxial 7	9.9	0.3	3.1	47.7	38.9

Table 14. Identification Results for a Uniform SB Model Fitted into the Observed Bridge Transverse Response with 5% Damping for AT6 – ST2

		Fitted Shear Beam into Bridge Transverse Response (Band-pass filtered **0–3.5** Hz)				
	Event	c [m/s]	σ_c [m/s]	$\frac{\sigma_c}{c}$ %	NRMSE %	$\Delta c/c$ %
AT6 – ST2	Biaxial 1	16.1	0.1	0.8	35.0	0.0
	Biaxial 2	13.9	0.5	3.4	63.2	13.6
	Biaxial 3	13.6	0.4	3.0	55.4	15.5
	Biaxial 4	11.6	0.4	3.1	43.8	27.8
	Biaxial 5	12.3	0.5	3.9	56.9	23.7
	Biaxial 6	11.3	0.5	4.8	61.2	29.8
	Biaxial 7	8.7	0.1	1.5	44.7	45.9

Table 15. Identification Results for a Uniform SB Model Fitted into the Observed Bridge Transverse Response with 5% Damping for AT6 – ST1

		Fitted Shear Beam into Bridge Transverse Response (Band-pass filtered **0–3.5** Hz)				
	Event	c [m/s]	σ_c [m/s]	$\frac{\sigma_c}{c}$ %	NRMSE %	$\Delta c/c$ %
AT6 – ST1	Biaxial 1	15.1	0.5	3.1	150.2	0.0
	Biaxial 2	14.3	0.4	3.1	61.6	5.1
	Biaxial 3	13.5	0.4	3.2	57.7	10.6
	Biaxial 4	11.3	0.4	3.3	45.1	25.1
	Biaxial 5	12.3	0.5	4.1	56.9	18.6
	Biaxial 6	10.9	0.5	4.7	60.1	27.8
	Biaxial 7	8.7	0.1	1.3	44.8	42.0

Table 16. Identification Results for a Uniform SB Model Fitted into the Observed Bridge Transverse Response with 5% Damping for AT8 – ST1

		Fitted Shear Beam into Bridge Transverse Response (Band-pass filtered **0–3.5** Hz)				
	Event	c [m/s]	σ_c [m/s]	$\frac{\sigma_c}{c}$ %	NRMSE %	$\Delta c/c$ %
AT8 – ST1	Biaxial 1	18.0	0.7	3.8	379.0*	0.0
	Biaxial 2	14.9	0.3	2.3	65.4	17.1
	Biaxial 3	15.3	0.3	2.2	78.5	14.6
	Biaxial 4	12.4	0.3	2.5	47.7	31.1
	Biaxial 5	11.4	0.4	3.6	47.2	36.8
	Biaxial 6	10.8	0.4	4.1	51.5	40.0
	Biaxial 7	10.9	0.6	5.3	59.4	39.4

* The normalized root mean square for this biaxial is considered as an outlier.

Fundamental frequency of vibration for structures (i.e., bridges or buildings) is a popular damage-sensitive parameter among researchers. The modal frequencies are considered a global dynamic characteristic of a structure which can be an indicator of overall damage in a structure. In this study, the researchers plotted the transfer function (TF) of the recorded response on the actual tested bridge (deck level with respect to base of columns) and read the apparent fundamental mode of vibration in the transverse direction. The apparent fundamental frequency for the three pairs of scenario I and for all the biaxial motions was read by plotting the transfer functions on top of each other. The three pairs of sensors were AT3 – ST3, AT5 – ST2, and AT7 – ST1. An approximate bell-shaped curve was passed through the fundamental mode of the transverse direction to help with reading for the first mode. Figure 47 shows the stacked plots of the transfer functions.

Figure 47 (multiple pages). Observed Change in Mode 1, Transverse Direction during Different Biaxial Motions

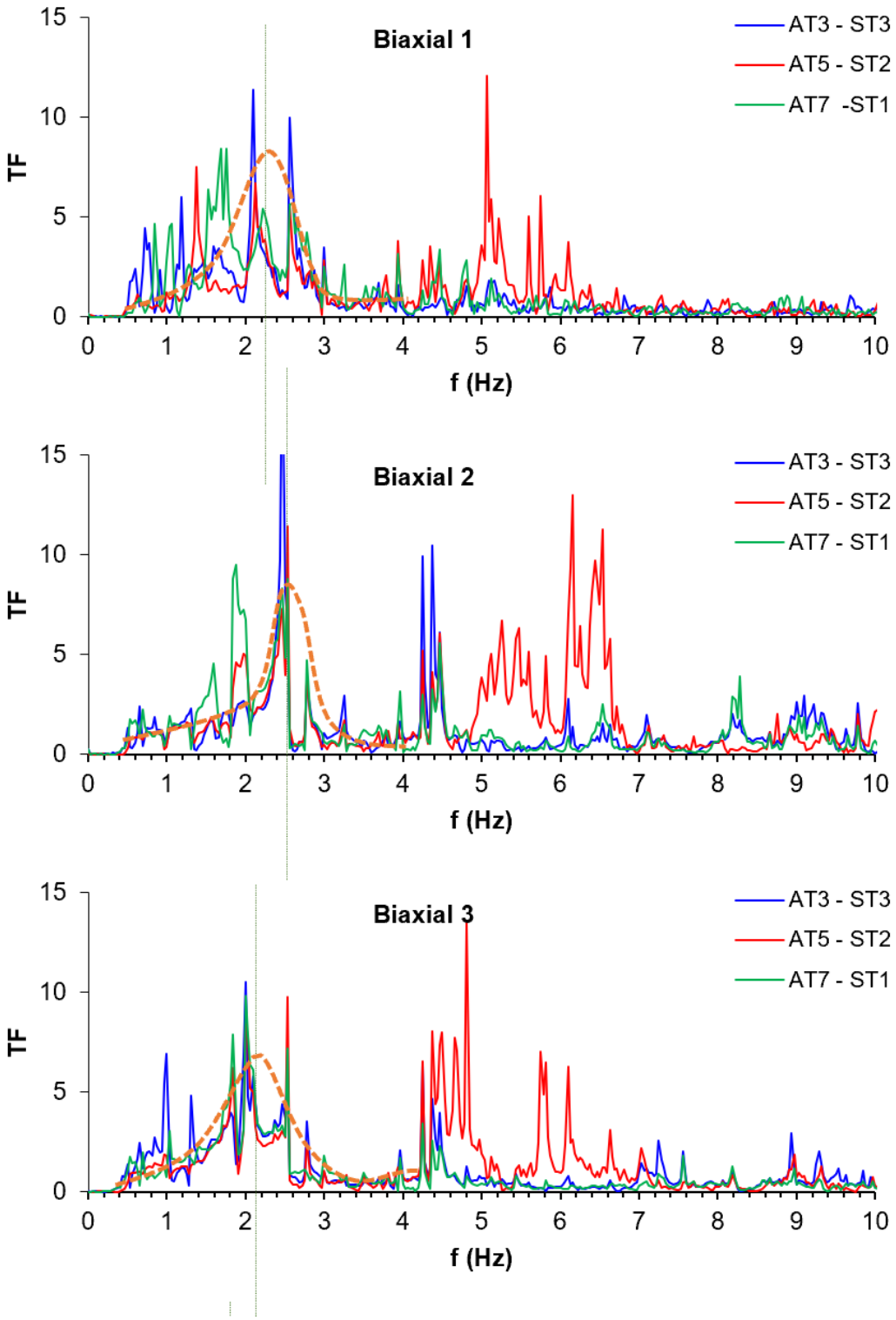

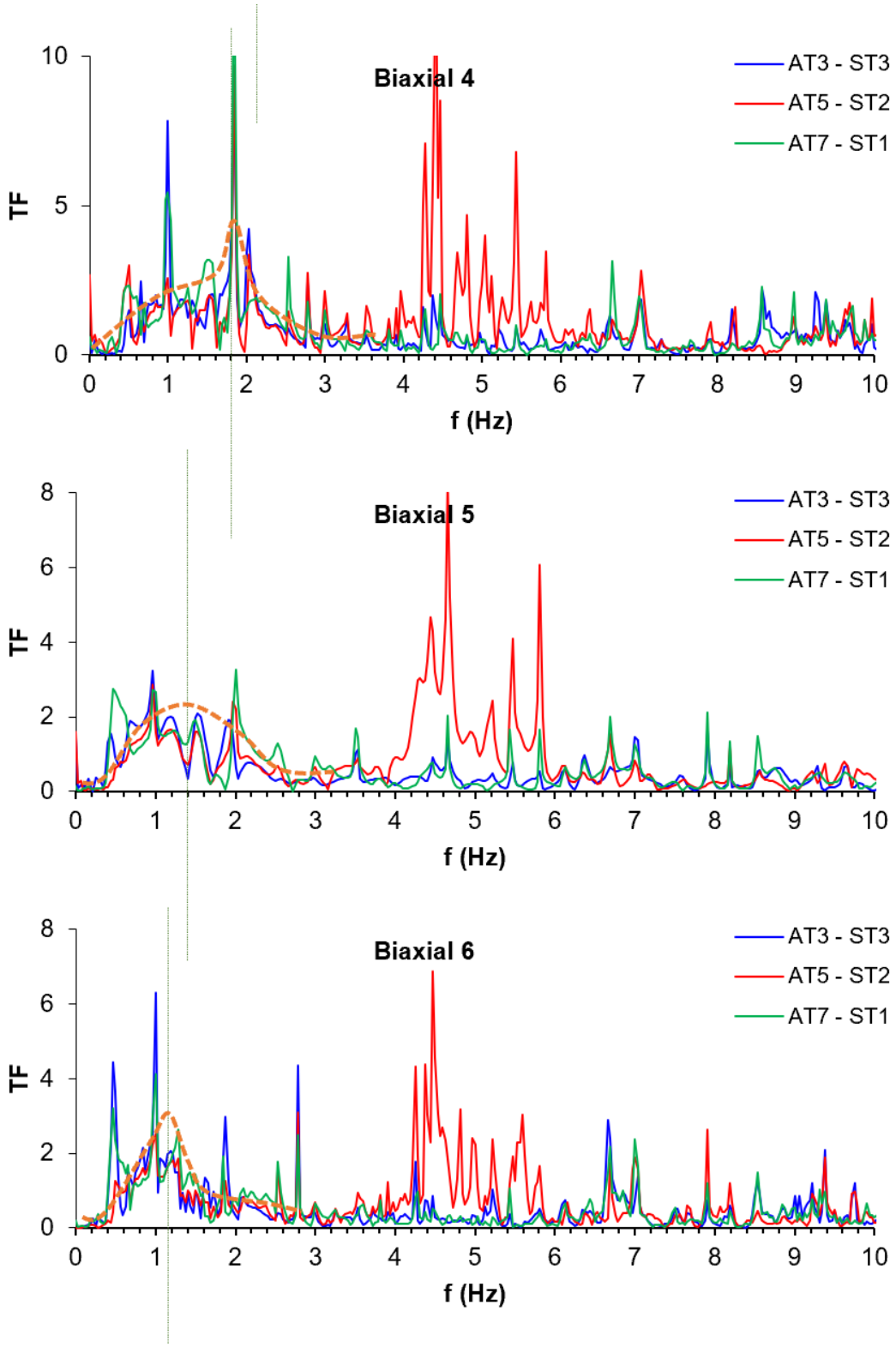
Biaxial 4
AT3 - ST3
AT5 - ST2
AT7 - ST1
TF
f (Hz)
Biaxial 5
AT3 - ST3
AT5 - ST2
AT7 - ST1
TF
f (Hz)
Biaxial 6
AT3 - ST3
AT5 - ST2
AT7 - ST1
TF
f (Hz)

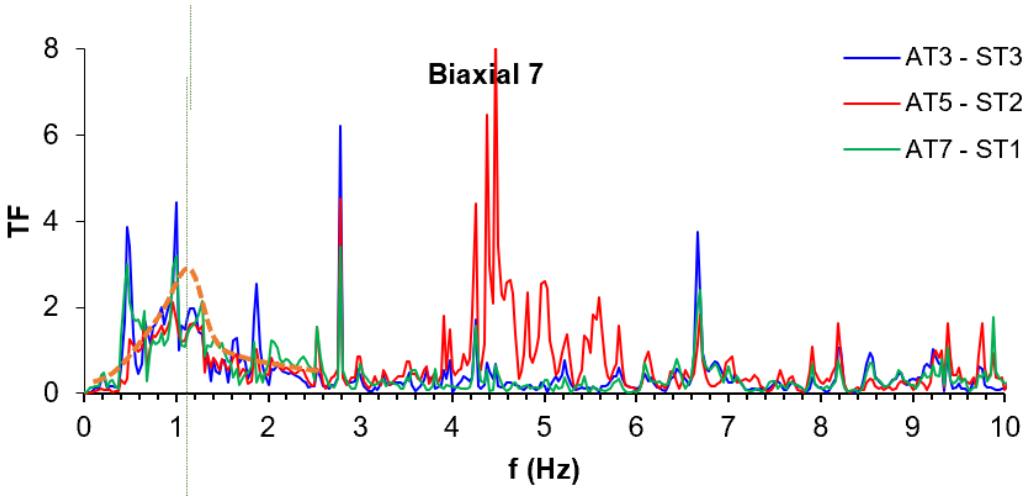

The percentage change in the frequency was calculated with frequency during Biaxial 1 as the benchmark. Table 17 gives an idea of how much the fundamental frequency changes from one motion to another.

Table 17. Observed Change in the Fundamental Mode, Transverse Direction

	Apparent Frequency	
Event	f_{1app} [Hz]	$\Delta f/f$ %
Biaxial 1	2.25	0.0
Biaxial 2	2.50	11.1
Biaxial 3	2.15	4.4
Biaxial 4	1.80	20.0
Biaxial 5	1.40	37.8
Biaxial 6	1.15	48.9
Biaxial 7	1.10	51.1

4.4 A Comprehensive Comparison of Identified Velocities and Their Changes with Actual Damage in the Bridge

A Detailed Damage Survey of the Bridge Structure after Each Major Shaking

This section primarily focuses on comparing reductions in the estimated shear wave velocities with the actual damage observed in the bridge. This comparison aids in understanding the accuracy of the wave method in detecting the actual damage in the bridge and the method's ability to localize it. It also helps identify limitations and benefits of using a shear beam model for the present wave-based approach. In summary, this section's comparisons and discussions shed light on the feasibility of the wave method and shear beam models for damage detection in a bridge structure.

Table 18 provides information regarding various damage states defined for bridges compiled from a report (Vosooghi and Saiidi 2010) and a guideline (Caltrans Design Criteria 2019). The information from this table will be used along with the visual damage description survey after each biaxial motion and for each bent. Visual damage description tables are summarized from the report by Nelson et al. (2007). The tables show information on the cracking, spalling, yielding, transverse drift ratio, and damage state condition of each bent (i.e., two columns).

Table 18. Damage-Defining Criteria of Bridges

Damage State [2]	DS-1: Flexural Cracks	DS-2: First Spalling and Shear Cracks	DS-3: Extensive Cracks and Spalling	DS-4: Visible Lateral and Longitudinal Bars	DS-5: Imminent Failure
Maximum drift ratio (%)	1.4–2.3	2.4–3.5	3.3–5.4	4.5–6.7	5.1–9.7
Damage State [3]	Minimal damage	Minimal damage	Moderate damage	Moderate damage	Major damage
Service Level [3]	Limited service, days	Limited service, days	Limited service, weeks	Limited service, weeks	No service

[2]: Vosooghi and Saiidi 2010; [3]: Caltrans Design Criteria 2019

The values of the reduction of shear wave velocities presented in Tables 19 to 21 are the respective averages of three pairs of sensors (i.e., scenario I and II) near each bent. These tables' rows present the damage states which correspond to the magnitude of the base motions (i.e., biaxials). Figures 48 through 50 are adopted from Nelson and Saiidi (2007).

Table 19. Summary of Damage Survey of Test Structure after each Earthquake Event for Pairs around Bent 1

	Damage State	Damage Description	Average Reduction of c (%)
Bent 1 AT6 – ST1, AT7 – ST1, AT8 – ST1	**Biax1**:	Visible cracking on the east top column, no spalling of concrete and no yielding or exposure of rebar as shown in Fig. 48 (a). No damage to nearby deck [1]. Transverse Drift Ratio approximately 1.1% (max. displacement of 17.3 mm in the transverse direction and 5.3 mm in the longitudinal direction). Damage state is considered *DS-1* per [2]. *Minimal* damage, falls within limited service-days per [3].	0
	Biax2:	Visible cracking on the east top column, no spalling of concrete and no yielding or exposure of rebar. No damage to nearby deck [1]. Transverse Drift Ratio approximately 0.8% (max. displacement of 11.9 mm in the transverse direction and 30 mm in the longitudinal direction). Damage state is considered *DS-1* per [2]. *Minimal* damage, falls within limited service-days per [3].	10.5
	Biax3:	Visible cracking on the columns, flake spalling of concrete and no yielding or exposure of rebar. No damage to nearby deck [1]. Transverse Drift Ratio approximately 1.43% (max. displacement of 21.8 mm in the transverse direction and 73.7 mm in the longitudinal direction). Damage state is considered *DS-1* per [2]. *Minimal* damage, falls within limited service-days per [3].	13.2
	Biax4:	Hairline cracking on the columns, one-fourth circular spalling of concrete on the bottom hinges of the columns, exposure of two lateral bars and no yielding as shown in Fig. 48 (b). No damage to nearby deck [1]. Transverse Drift Ratio approximately 2.6% (max. displacement of 39.9 mm in the transverse direction and 77.5 mm in the longitudinal direction). Damage state is considered *DS-2* per [2]. *Moderate* damage, falls within limited service-weeks per [3].	28.7
	Biax5:	Hairline cracking on the columns, three-fourths circular spalling of concrete on the bottom hinges of the west column, exposure of three lateral bars on top of east column and eight lateral bars on both bottom of both columns. The rebar yielding increased. No damage to nearby deck [1]. Transverse Drift Ratio approximately 3.9% (max. displacement of 59.9 mm in the transverse direction and 91.2 mm in the longitudinal direction). Damage state is considered *DS-3* per [2]. *Moderate* damage, falls within limited service-weeks per [3].	28.0
	Biax6:	Widespread cracking on the columns, three-fourth spalling of concrete on the bottom hinges of both columns, exposure of almost all longitudinal bars in both columns. No damage to nearby deck [1]. Transverse Drift Ratio approximately 7.6% (max. displacement of 115.8 mm in the transverse direction and 101.1 mm in the longitudinal direction). Damage state is considered *DS-5* per [2]. *Major* damage, falls within no service per [3].	34.1
	Biax7:	Dense cracking on the columns, whole circular spalling of concrete on the bottom hinges of both columns, exposure of all the longitudinal bars and eight lateral bars, all other bars are buckled as shown in Fig. 48 (c). No damage to nearby deck [1]. Transverse Drift Ratio approximately 8.84%. Damage state is considered *DS-5* per [2]. *Major* damage, falls within no service per [3].	38.3

[1]: Nelson and Saiidi 2007; [2]: Vosooghi and Saiidi 2010; [3]: Caltrans Design Criteria

Figure 48. Damage Progression in Bent 1 during Biaxial 1 (a), Biaxial 4 (b), and Biaxial 7 (c)

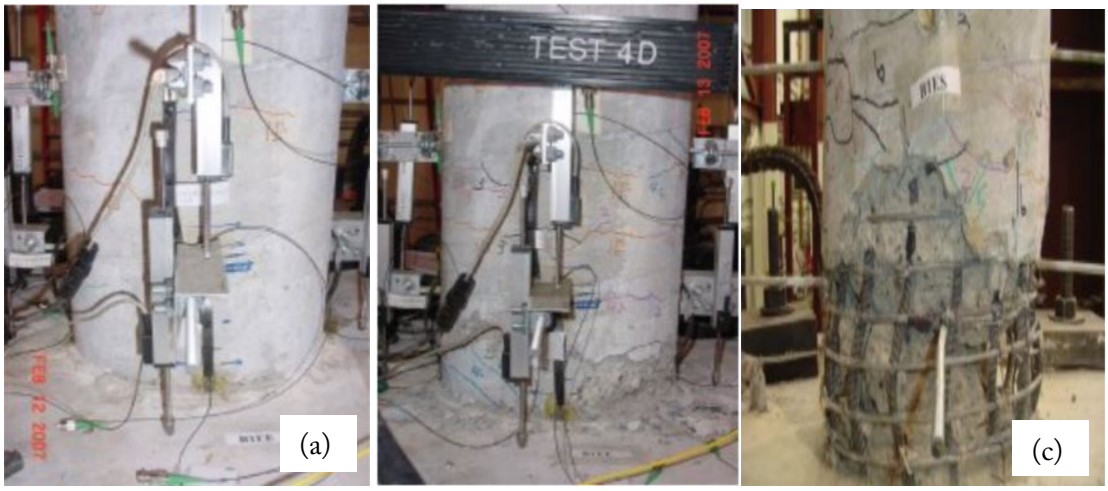

Figure 49. Damage Progression in Bent 2 during Biaxial 1 (a), Biaxial 4 (b), and Biaxial 7 (c)

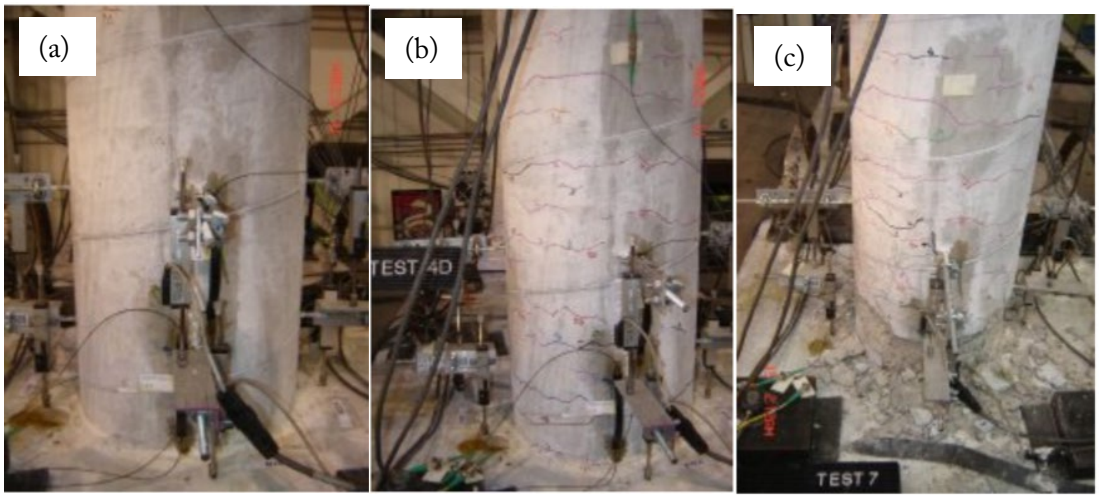

Figure 50. Damage Progression in Bent 3 during Biaxial 1 (a), Biaxial 4 (b), and Biaxial 7 (c)

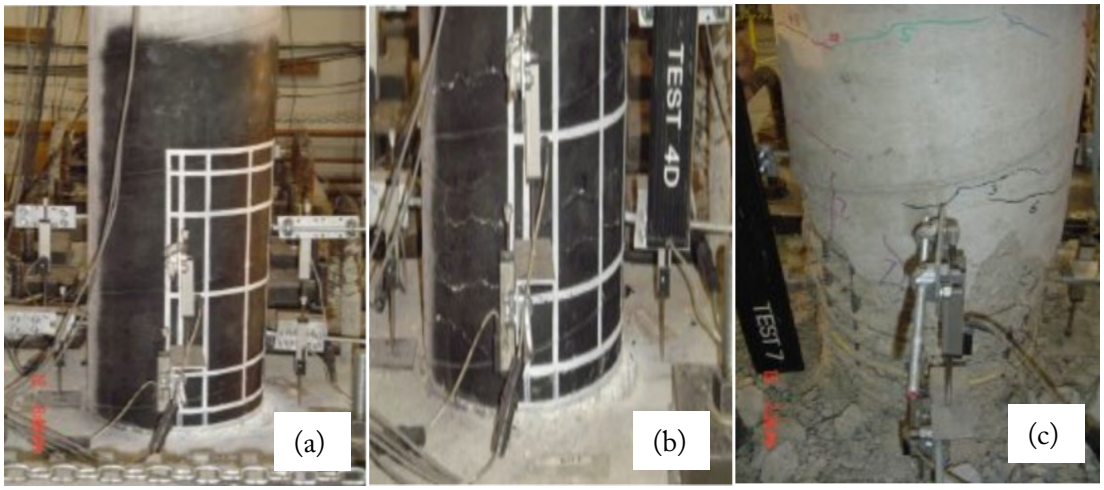

Table 20. Summary of Damage Survey of Test Structure after each Earthquake Event for Pairs around Bent 2

	Damage State	Damage Description	Average Reduction of *c* (%)
Bent 2 AT4 - ST2, AT5 – ST2, AT6 - ST2	**Biax1**:	No visible cracking on the columns, no spalling of concrete and no yielding or exposure of rebar as shown in Fig. 49 (a). No damage to nearby deck [1]. Transverse Drift Ratio approximately 0.3% (max. displacement of 6.6 mm in the transverse direction and 5.3 mm in the longitudinal direction). Damage state is considered *DS-1* per [2]. *Minimal* damage, falls within limited service-days per [3].	0
	Biax2:	No visible cracking on the columns, no spalling of concrete and no yielding or exposure of rebar. No damage to nearby deck [1]. Transverse Drift Ratio approximately 0.4% (max. displacement of 9.4 mm in the transverse direction and 30 mm in the longitudinal direction). Damage state is considered *DS-1* per [2]. *Minimal* damage, falls within limited service-days per [3].	9.5
	Biax3:	No visible cracking on the columns, no spalling of concrete and no yielding or exposure of rebar. No damage to nearby deck [1]. Transverse Drift Ratio approximately 0.9% (max. displacement of 19.1 mm in the transverse direction and 73.7 mm in the longitudinal direction). Damage state is considered *DS-1* per [2]. *Minimal* damage, falls within limited service-days per [3].	12
	Biax4:	Hairline cracking on the columns, no spalling of concrete and no yielding or exposure of rebar as shown in Fig. 49 (b). No damage to nearby deck [1]. Transverse Drift Ratio approximately 1.5% (max. displacement of 31 mm in the transverse direction and 77.5 mm in the longitudinal direction). Damage state is considered *DS-1* per [2]. *Minimal* damage, falls within limited service-days per [3].	26.8
	Biax5:	Hairline cracking on the columns, minor flake spalling of concrete, no exposure and yielding of rebar. No damage to nearby deck [1]. Transverse Drift Ratio approximately 1.8% (max. displacement of 39.4 mm in the transverse direction and 91.2 mm in the longitudinal direction). Damage state is considered *DS-1* per [2]. *Minimal* damage, falls within limited service-days per [3].	29.0
	Biax6:	Hairline cracking on the columns, half circular spalling of concrete on the bottom hinge of east column, slight yielding, exposure of three lateral rebars. No damage to nearby deck [1]. Transverse Drift Ratio approximately 2.8% (max. displacement of 60.2 mm in the transverse direction and 101.1 mm in the longitudinal direction). Damage state is considered *DS-2* per [2]. *Minimal* damage, falls within limited service-days per [3].	36.0
	Biax7:	Widespread cracking on the columns, half circular spalling of concrete on the bottom hinges of both columns and slight yielding, four exposure of lateral bars as shown in Fig. 49 (c). No damage to nearby deck [1]. Transverse Drift Ratio approximately 3.22%. Damage state is considered *DS-2* per [2]. *Minimal* damage, falls within limited service-days per [3].	42.8

[1]: Nelson and Saiidi 2007; [2]: Vosooghi and Saiidi 2010; [3]: Caltrans Design Criteria

Table 21. Summary of Damage Survey of Test Structure after each Earthquake Event for Pairs around Bent 3

	Damage State	Damage Description	Average Reduction of *c* (%)
Bent 3 AT2 – ST3, AT3 – ST3, AT4 – ST3	**Biax1**:	No visible cracking on the columns, no spalling of concrete and no yielding or exposure of rebar as shown in Fig. 50 (a). No damage to nearby deck [1]. Transverse Drift Ratio approximately 0.9% (max. displacement of 16.8 mm in the transverse direction and 5.3 mm in the longitudinal direction). Damage state is considered *DS-1* per [2]. *Minimal* damage, falls within limited service-days per [3].	0
	Biax2:	No visible cracking on the columns, no spalling of concrete and no yielding or exposure of rebar. No damage to nearby deck [1]. Transverse Drift Ratio approximately 0.8% (max. displacement of 14 mm in the transverse direction and 30 mm in the longitudinal direction). Damage state is considered *DS-1* per [2]. *Minimal* damage, falls within limited service-days per [3].	3.3
	Biax3:	No visible cracking on the columns, no spalling of concrete and no yielding or exposure of rebar. No damage to nearby deck [1]. Transverse Drift Ratio approximately 1.4% (max. displacement of 24.9 mm in the transverse direction and 73.7 mm in the longitudinal direction). Damage state is considered *DS-1* per [2]. *Minimal* damage, falls within limited service-days per [3].	5.1
	Biax4:	Hairline cracking on the columns, half circular spalling of concrete on the bottom hinge of the west column, no yielding of bars, exposure of three rebars as shown in Fig. 50 (b). No damage to nearby deck [1]. Transverse Drift Ratio approximately 2.7% (max. displacement of 49.5 mm in the transverse direction and 77.5 mm in the longitudinal direction). Damage state is considered *DS-2* per [2]. *Minimal* damage, falls within limited service-days per [3].	22.4
	Biax5:	Hairline cracking on the columns, half circular spalling of concrete on the bottom hinge of the west column, exposure of six lateral and one longitudinal rebars. No damage to nearby deck [1]. Transverse Drift Ratio approximately 4.4% (max. displacement of 80.5 mm in the transverse direction and 91.2 mm in the longitudinal direction). Damage state is considered *DS-3* per [2]. *Moderate* damage, falls within limited service-weeks per [3].	27.1
	Biax6:	Widespread cracking on the columns, half circular spalling of concrete on the bottom hinges of both the columns, exposure of eight lateral and three longitudinal rebars. No damage to nearby deck [1]. Transverse Drift Ratio approximately 7.0% (max. displacement of 127.5 mm in the transverse direction and 101.1 mm in the longitudinal direction). Damage state is considered *DS-5* per [2]. *Major* damage, falls within no service per [3].	29.6
	Biax7:	Widespread cracking of columns, three-fourth circular spalling of concrete on the bottom hinge of the west column, exposure of nine lateral and 11 longitudinal rebars with one incipient buckling as shown in Fig. 50 (c). No damage to nearby deck [1]. Transverse Drift Ratio approximately 7.4%. Damage state is considered *DS-5* per [2]. *Major* damage, falls within no service per [3].	33.2

[1]: Nelson and Saiidi 2007; [2]: Vosooghi and Saiidi 2010; [3]: Caltrans Design Criteria 2019

A Correlation between Detected Changes in the Velocities and the Actual Damage in the Bridge

This section mainly discusses the observed trends in the estimated shear wave velocities, their percentage changes, and their correlation with the surveyed damage discussed in the previous section. When the bridge was excited by shake-table motions with higher amplitudes in each test, each bent sustained different damages. According to the damage survey (Nelson et al. 2007), Bent 1, being the shortest bent and close to the south abutment, experienced the maximum damage during the shake-table tests. Bent 3 was subjected to less damage and experienced moderate damage. Bent 2 was the tallest bent among the three, and it experienced the least damage. The observed damage states in Tables 19 to 21 were compared with the average reduction of shear wave velocity in the bridge and near each bent. The goal was to determine whether (1) the reduction trend in the velocity was consistent with actual damage in the bridge, and (2) the damage was localized. Figure 51 compares the reduction of estimated shear wave velocity and the actual damage state in the bridge.

Figure 51. Comparison between (a) Average Reduction of Shear Wave Velocity and (b) Actual Damage in the Bridge

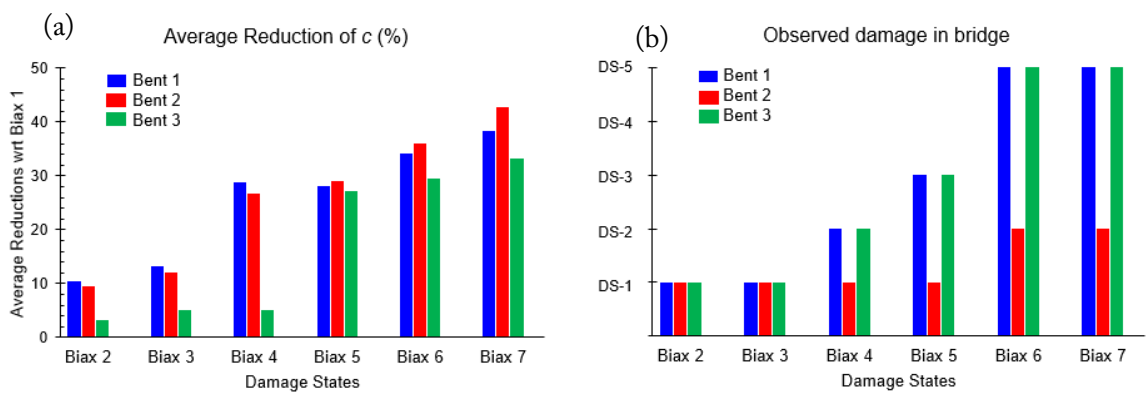

The very first motion (Biaxial 1), during which the bridge remained elastic, was used as the baseline for calculating percentage reduction in the velocities. Hence, Figure 51a shows the relative percentage reductions for biaxial motions 2 through 7. The average reductions in the shear wave velocities are then compared with observed extent of damage in the bridge. Figure 51b presents the level of actual damage observed in the bents of the tested bridge according to on-site surveys (Tables 19 to 21). Figure 51b shows that the damage state indices up to Biaxial 3 are consistently ranked as DS-1 for all three bents, as there was no damage or very minor damage in the columns of the bridge. There is a change in the damage state indices for Bents 1 and 3 during Biaxial 3, Biaxial 4, and Biaxial 5. Bent 2 remains negligibly damaged (i.e., DS-1) up to Biaxial 5. However, there is a change of damage state for bent 2 during Biaxial 6 and 7. As these damage state indices are based on the transverse drift ratio, one can notice that the damage states for Bent 1 and Bent 3 are similar. However, there is a difference in their drift values and their sustained damages in the tested bridge. Bent 1 has sustained slightly larger damage than Bent 3. Hence, the average reductions (the heights of the bars) depicted in Figure 51b should be considered as a rating for the

sustained damage rather than an exact damage indication. Comparing the trends in Figure 51a and 51b, the overall change in the velocities (i.e., an average of the three bents) is consistent with the actual sustained damage in the bridge. In other words, the velocity reductions for biaxial motions 1 and 3 are the least, while the magnitude of change increases consistently from biaxial motions 4 to 7. Figure 52 presents the average reduction in the estimated shear wave velocities for all three bents. The trend is consistent with the surveyed damage for the bents (Figure 51b and Tables 19 to 21).

Figure 52. Average Reduction of Shear Wave Velocities for the Three Bents

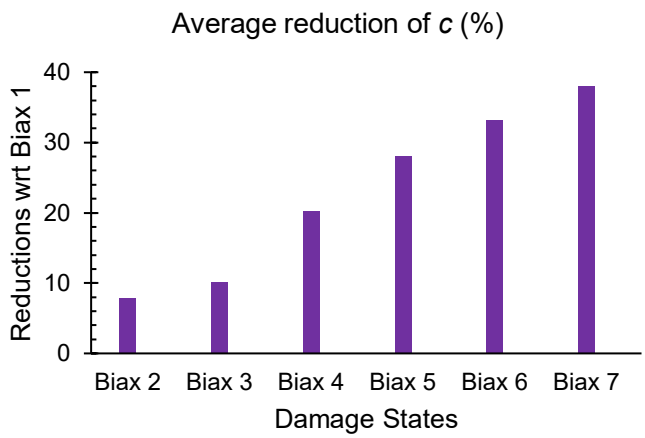

Figure 53. Comparison between the Average Reduction in Shear Wave Velocity and the Reduction in the Apparent Transverse Frequency of the Bridge

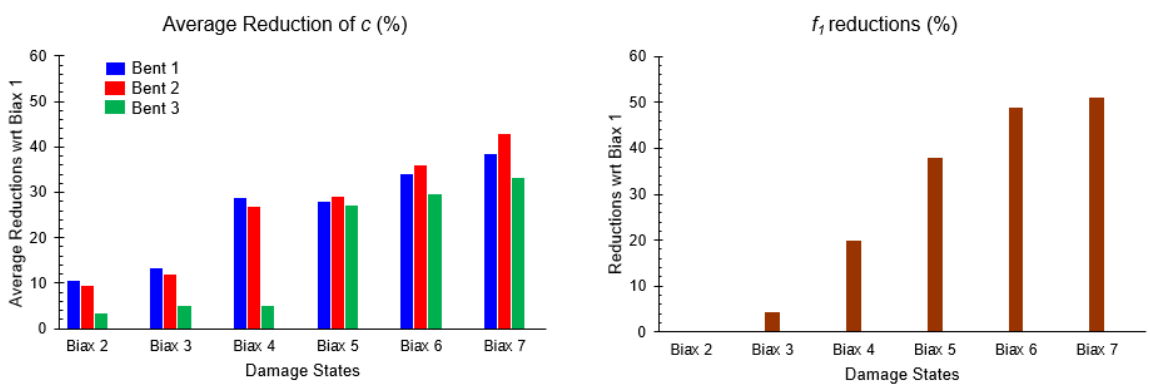

In addition, the authors drew a comparison between the average reduction in the velocities and the change in apparent fundamental frequencies. The apparent frequencies were read from the transfer function of the bridge response during actual testing of the bridge, as discussed in the previous section. The percentage reductions in the frequencies were calculated with respect to the first event, Biaxial 1. The frequency of a structure is reduced if its mass increases or its stiffness decreases. The

bridge mass remained the same throughout the tests; therefore, the percentage reduction in the apparent frequencies can be related to damage in the bridge. Figure 53 shows the side-by-side comparison. The results show that the average percentage reductions in the velocities are consistent with reductions in the frequencies. Both plots present an increasing change, consistent with the overall observed damage in the bridge. The apparent frequency of vibration is a global characteristic of the structure which is limited to detecting global changes in the structure and cannot localize the damage. The wave method presented in this study can be sensitive to local damages. However, the results in Figures 51 to 53 reveal that the method could not localize damage in the case study bridge while the global changes were detected reasonably well. In the next chapter, the authors discuss the feasibility of this method for detecting and localizing damage in the bridges and explore root causes for its limitations observed in this study. Furthermore, recommendations will be provided for developing the method to improve its accuracy and robustness in detecting and localizing damage in bridges.

V. Conclusions

This study extended the application of the wave method for structural health monitoring (SHM) to bridge structures. The research team aimed to explore the feasibility of the method for SHM in bridges—in both accurately detecting damage and localizing it along the bridge length. The researchers used the wave method to identify dynamic characteristics of the case-study bridge using wave propagation in a simple uniform shear beam model. The method identifies a wave velocity for the structure by fitting an equivalent uniform shear beam model to the recorded earthquake response. The structural damage is inferred by detecting changes in the identified velocities from one damaging event to another. For simplicity, only the transverse response of the bridge was utilized in this study. There were nine accelerometers on the bridge deck and three at the shake-table level. To identify the bridge's structure, data from two sensors are required: one from the deck and one from the base. Hence, several wave paths were defined and categorized in two scenarios. The identified shear wave velocities for each scenario and seven shaking intensities were reported and a summary of the observed actual damages in the structure presented. The observed damages were grouped into seven damage states which were further compared with the reductions in the identified velocities and the apparent frequencies. Referring to the results presented in the previous sections, the main findings are as follows.

- The identified shear wave velocities presented a decreasing trend as the shaking intensity was increased. This was the case for both wave passage scenarios.
- The *average* percent reduction in the velocities was consistent with the overall observed damage in the bridge. This implies that the wave method is a feasible method for detecting the overall damage in a bridge structure.
- There was no correlation between the estimated reduction in the velocity for a given bent and its actual sustained damage during the seven motions. This reveals that the wave method, using a simple uniform shear beam model, was unable to localize damage in the bridge. In other words, it did not identify which column (i.e., bent) sustained the most damage. This indicates that the uniform shear beam model is too simple to localize the damage in the bridge. The model rather provides a proxy on the extent of overall change in the bridge response due to damage.
- The main reason for not being able to localize the damage is that the bridge response (deck and columns) is mainly in bending, while the shear beam model only moves in shear (i.e., no flexural motion). Bending motion leads to wave dispersion in the bridge (i.e., waves propagate with different speeds at different frequencies). Wave dispersion results in distortion of the main pulses in the impulse response functions (IRFs) as well as causing a time shift in the pulses. These effects directly impact the identified shear wave velocities simply because the shear beam model's IRFs are not affected by dispersion. Therefore, a more detailed model must take into account the bending

nature of the bridge response and the significant wave dispersion associated with it. For example, a Timoshenko beam model, which moves in both bending and shear, can be used for the identification. While the shear beam model provided a unique opportunity for extending the wave method application to a bridge structure, further research will be needed to develop and calibrate a more detailed model for the purpose of robust damage detection and damage localization in bridges.

This study, as the first step in developing the wave method for bridge structural health monitoring, has shown promising results in detecting the overall damage. Therefore, it is expected that a more complex wave propagation model (e.g., a Timoshenko beam) with ability of capturing the bending motions at the bridge deck and piers, will improve the spatial accuracy of the structural identification and its capacity for damage localization.

List of Abbreviations

SHM	Structural Health Monitoring
FEM	Finite Element Model
TF	Transfer Function
IRF	Impulse Response Function
wrt	with respect to
TH	Time History
SB	Shear Beam

Bibliography

Benzoni, G., N. Bonessio, and G. Lomiento. "Structural Health Monitoring of Bridges with Seismic Response Modification Devices." Report No. SSRP-13/02. University of California, San Diego, Department of Structural Engineering, 2013.

Caltrans. "Caltrans Seismic Design Criteria Version 2.0." State of California, Department of Transportation, 2019.

Chopra, A. K. *Dynamics of Structures: Theory and Applications to Earthquake Engineering*. Pearson: Hoboken, NJ, 2017.

DeedShub. "Seismic Performance of Bridge Systems with Conventional and Innovative Materials (NEES-2005-0033). "Experiment-1: Four-span Bridge Biaxial Shake-Table Experiments – Phase I – Conventional Bridge." https://datacenterhub.org/dv_dibbs/view/1322:dibbs/experiments_dv/.

Feng, M. Q., and D. K. Kim. "Long-Term Structural Performance Monitoring of Two Highway Bridges, Phase I: Instrumentation." RTA-59A0155. University of California, Irvine, Department of Civil and Environmental Engineering, 2001.

Feng, M. Q., Y. Fukuda, X. Deng, Y. Guan, and H. Gomez. "Long-Term Structural Performance Monitoring of Bridges." University of California, Irvine, Department of Civil and Environmental Engineering, 2011.

Feng, M. Q., Y. Fukuda, Y. Chen, S. Soyoz, and S. Lee. "Long-Term Monitoring of Bridges, Phase II: Development of Baseline Model and Methodology for Health Monitoring and Damage Assessment." Report No. CA07-0245. University of California, Irvine, Department of Civil and Environmental Engineering, 2008.

Isakovic, T., M. Saiidi, and M. Fischinger. "Numerical Modelling of a Four-Span Bridge, Bi-Axially Tested on Three Shake Tables." Fourth ECCOMAS Thematic Conference on Computational Methods in Structural Dynamics and Earthquake Engineering (2013), Kos Island, Greece.

Levenberg, K. "A Method for the Solution of Certain Non-Linear Problems in Least Squares." *The Quarterly of Applied Mathematics* 2 (1944): 164–168.

Marquardt, D. W. "An Algorithm for Least-Squares Estimation of Nonlinear Parameters." *Journal of the Society for Industrial and Applied Mathematics* 11, no. 2 (1963): 431–441.

Nelson, R. B., M. Saiidi, and S. Zadeh. "Experimental Evaluation of Performance of Conventional Bridge Systems." Report No. CCEER-07-04. Centre for Civil Engineering Earthquake Research, Department of Civil and Environmental Engineering, University of Nevada (Reno, NV), 2007.

Rahmani M., and M. I. Todorovska. "1D system identification of buildings from earthquake response by seismic interferometry with waveform inversion of impulse responses: Method and application to Millikan Library." *Soil Dynamic Earthquake Engineering*, Jose Roësset Special Issue. E. Kausel and J. E. Luco (Guest Editors), 47 (2013): 157–174. DOI: 10.1016/j.soildyn.2012.09.014.

Rahmani, M., and M. I. Todorovska. "Structural Health Monitoring of a 54-Story Steel-Frame Building Using a Wave Method and Earthquake Records." *Earthquake Spectra* 31, no. 1 (2015): 501–525. DOI: 10.1193/112912EQS339M.

Rahmani, M., M. Ebrahimian, and M. I. Todorovska. "Time-Wave Velocity Analysis for Early Earthquake Damage Detection in Buildings: Application to a Damaged Full-Scale RC Building." *Earthquake Engineering and Structural Dynamics* 44, no. 4 (2015): 619–636. DOI: 10.1002/eqe.2539

Saiidi, M., A. Vosooghi, and R. B. Nelson. "Post-Earthquake Evaluation and Emergency Repair of Damaged RC Bridge Columns Using CFRP Materials." Report No. CCEER-10-05. Center for Civil Engineering Earthquake Research, Department of Civil Engineering, University of Nevada (Reno, NV), 2010.

Saiidi, M., A. Vosooghi, and R. B. Nelson. "Shake-Table Studies of a Four-Span Reinforced Concrete Bridge." American Society of Civil Engineers, 2013. DOI: 10.1061/(ASCE)ST.1943-541X.0000790

Todorovska, M. I., and M. Rahmani. "System Identification of Buildings by Wave Travel Time Analysis and Layered Shear Beam Models: Spatial Resolution and Accuracy." *Journal of Structural Control and Health Monitoring* 20, no. 5 (2012): 686–702, DOI: 10.1002/stc.1484 (2012).

Vosooghi, A., and M. Saiidi. "Seismic Damage States and Response Parameters for Bridge Columns." ACI Special Publications, SP271-02. Structural Concrete in Performance-Based Seismic Design of Bridges, 271 (2010), 29–46.

About the Authors

Mehran Rahmani, PhD, PE (Principal Investigator)

Dr. Mehran Rahmani is an assistant professor in the Civil Engineering Construction Engineering Management (CECEM) department at California State University, Long Beach (CSULB). He earned his PhD in Structural and Earthquake Engineering from the University of Southern California (USC) in 2014, his MS in Electrical Engineering (with an emphasis on signal processing) from USC in 2013, and his MS in Structural Engineering from Sharif University of Technology (Iran) in 2009. Prior to joining CSULB, Dr. Rahmani, a registered Professional Engineer (PE) in the State of California, worked as a Senior Engineer and a Project Engineer in the structural engineering industry from 2014–2017.

Dr. Rahmani's research focuses on structural system identification, structural health monitoring, and earthquake damage detection of buildings and bridges using sensory data. His PhD research was focused on developing a wave-based methodology for remote post-earthquake structural damage detection that is robust when applied to actual structures and calibrated using data from full-scale buildings. His PhD research was funded by NSF (CMMI-0800399). He has been instrumental in advances in wave-based structural identification and monitoring in the past ten years, receiving more than 300 citations for his technical papers.

Manan Naik, MSCE, EIT (Graduate Research Assistant)

Manan Naik joined California State University, Long Beach as a graduate student in Fall 2017. He obtained his MS in Civil Engineering from CSULB in 2020 and his BS in Civil Engineering from Gujarat Technological University (India) in 2017. He is a certified Engineer-in-Training (EIT) in the State of California.

Naik was a graduate research assistant at California State University, Long Beach from 2018–2020. His responsibilities as a graduate student included performing computer modeling and analysis for structural systems for all types of bridges and materials using SAP2000, assisting with writing and running MATLAB programs to analyze sensory data in select bridges, preparing and writing summary reports, and preparing plots and spreadsheets for analysis results.

MTI FOUNDER

Hon. Norman Y. Mineta

MTI BOARD OF TRUSTEES

Directors

MINETA TRANSPORTATION INSTITUTE